3D groundwater flow in heterogeneous subsurfaces underneath dikes

FINAL VERSION

ing. Johannes de Groot

Department of Physical Geography
Utrecht University

3D groundwater flow in heterogeneous subsurfaces underneath dikes

FINAL VERSION

Date of submission	June 9, 2016
Author	ing. Johannes de Groot
Student number	4205057
Supervisors	dr. Esther Stouthamer
	dr. Kim Cohen
	dr. Rens van Beek
Institute	Department of Physical Geography
	Faculty of Geosciences
	Utrecht University

Abstract

Deltas often form the economic heart of countries and the foundation for social and agricultural activities. Dikes protect these valuable areas from flooding by rivers. The stability of dikes constructed in such areas is crucial in countries such as the Netherlands. This research focused on a specific type of dike failure named piping. Piping is a process in the subsurface and is divided into three phases:

1. A groundwater flow starts running from the river into a permeable layer (aquifer) towards the protected polder. The hydraulic head in the aquifer increases, resulting in upward pressure beneath the low permeable top layer.
2. The top layer breaches when the hydraulic head exceeds the critical hydraulic head. Such a breach forms a hydraulic connection between the aquifer and the surface, resulting in water flow towards the surface.
3. The water flow erodes a pipe directly beneath the top layer in the opposite direction of the groundwater flow. Continuous erosion may result in failure of the dike.

The current method to calculate piping contains three formulas to calculate each phase of the process [Föster et al., 2012]. The output is the minimal seepage length from the river towards the polder that is necessary to prevent piping. This method has a two-dimensional approach and fails to consider three-dimensional variations in the subsurface architecture and properties. In addition, the Sellmeijer formula that calculates the third phase has a large dependency on grain size.

The aim of this research was to investigate the behavior of groundwater flow in heterogeneous sub-surfaces (first phase) by using a three-dimensional groundwater model (iMOD) and visualize the risk for breaching of the top layer during a flood wave (second phase). Heterogeneity is implemented in the models by schematizing a fossil channel belt with varying properties on top of the thick aquifer. The results are compared with the results of the prescribed method for calculating piping [Föster et al., 2012].

The risk in days for breaching of the top layer during a flood wave is set as an indicator for the risk of piping. This risk depends on the properties of the channel belt. Situations with a narrow channel belt result in more risk (days) for breaching of the top layer compared to a wide channel belt. On the other hand, this risk for breaching of the top layer covers a larger area for wide channel belts, while the number of days with this risk is less. Considering channel belts that partly incise in the underlying aquifer, the risk for piping is larger than the traditional method for calculating piping suggests. The aquifer thickness is significantly less at the isolated part of a channel belt and therefore the calculations with Sellmeijer result in

small values for the required seepage length. At these locations, the groundwater flow is not induced by the connection of the channel belt with the river, but the incision nearby. A two-dimensional approach cannot take this in consideration. The results from three-dimensional calculations show a risk for breaching of the top layer located at the isolated part of the channel belt within the distance of the required seepage length. This will result in three-dimensional development of piping because the erosion moves in the direction of the largest hydraulic head. These results show that three-dimensional groundwater models like iMOD are a useful tool for investigating the behavior of groundwater flow underneath dikes in heterogeneous subsurfaces.

This research forms the foundation for further research to three-dimensional modeling of groundwater flow underneath dikes. Recommendations are formulated based on the results of this research and the available tools in iMOD. The first steps that should be made are:

- investigating the influence of a breached top layer in the polder on the hydraulic head;
- investigating the preferential paths of groundwater flow from the river towards a breach in the top layer through a heterogeneous subsurface.

Contents

Equations

Figures

Tables

1 Introduction

Deltas provide people with the benefits of logistical accessibility, drinking water and fertile soil for agriculture and pose a growing water management challenge. This is amplified by the worldwide growth in human populations in delta areas, such as the Rhine-Meuse delta. This leads to extensive infrastructure development but also increases the risk posed to populations in such areas given the constant threat of flooding from the rivers and the sea. In response, societies have invested considerable time and resources in the construction of dikes along the rivers and polders. These dikes are designed to protect low-lying areas from flooding and to regulate the flow of rivers. During a flood wave, the water level in the river rises and groundwater will seep from the river into permeable sand layers towards the polder. This influences the stability of the dikes with an increasing risk of failure. Therefore, the dikes must meet strict safety requirements for height and stability, which are set by the government. Geotechnical calculations are made for designing and testing of dikes in order to meet these safety requirements. A distinction is made between different forms of dike failure with a specific approach to confirm compliance with the requirements. This study focuses on one specific form of dike failure named piping.

1.1 Piping as a three-phase process

Vrijling et al. [2010] and Förster et al. [2012] give a detailed explanation of the process of piping and current predicting/designing methods. The process is divided in three phases: (1) groundwater flow from the river towards the polder, (2) bursting of the top layer followed by backward erosion (3) from the polder towards the river. A significant risk of dike failure as a result of piping is expected when all phases of this process take place in succession. This paragraph summarizes the three phases explained by these authors.

Phase 1: ground water flow and increasing water pressure.

Along a cross-section from an inundated floodplain, across the dike and to the protected polder, the hydraulic head of the upper groundwater system will increase as the water level in the river rises with the arrival of a flood wave (Figure 1.1). If the open channel of the river connects to a permeable sand body (aquifer), a groundwater flow will start running towards areas with a lower hydraulic head. The aquifer forms a hydraulic connection between the river and the polder, which is generally covered by a confining top layer (aquitard) of peat and/or clay. Groundwater barely flows through this poor permeable layer, resulting in increasing water pressure in the aquifer.

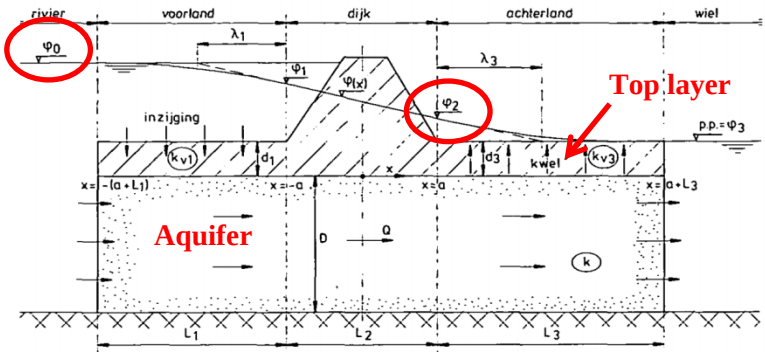

Figure 1.1 Schematic cross section of a dike with the parameters for calculating the hydraulic head [TAW, 1985].

Phase 2: breaching of the top layer.

The risk for breaching of the top layer depends on the weight of the top layer and upward water pressure induced by the water level in the river. The top layer becomes buoyant as the hydraulic head (ϕ) reaches the critical hydraulic head ($\phi_{z,g}$). As the hydraulic head exceeds the critical hydraulic head ($\phi > \phi_{z,g}$), the top layer will breach because the upward pressure is larger than the weight of the top layer. This results in a vertical hydraulic connection between the aquifer and the surface. Groundwater will flow through the breach towards the surface and a boil will appear. Note that a buoyant top layer in the direct vicinity of the dike also potentially reduces the stability of the dike, but this is considered as an independent way of potential dike failure, not failure due to piping.

Phase 3: backwards erosion.

The vertical water flow through the breached top layer erodes sand and brings it towards the surface (Figure 1.2). When such groundwater flow is sustained long enough, a horizontal pipe will form in the opposite direction of the groundwater flow (backward erosion). The hydraulic head will decrease as the pipe grows and the hydraulic resistance decreases. The erosion continues as the water level in the river keeps increasing. Continuous erosion could eventually result in failure of the dike.

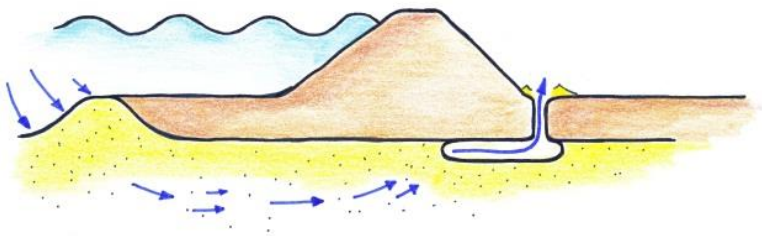

Figure 1.2 Backward erosion creates a pipe that can eventually result in a failure of the dike [Koopmans and Van den Berg, 2015].

1.2 Observations

Dike breaches due to piping have been observed in the past. During the high water event in 1926, a dike failed close to the village Zalk [Vrijling et al., 2010]. The inhabitants and employees of the water board observed a small boil at the inner toe of the dike. After a short period, the boil started to grow which resulted in a breach of the dike. During the high water events in 1993 and 1995, hundreds of small boils were seen along the dikes of all major rivers (Figure 1.3), but none developed in a dike breach [Rijkswaterstaat Projectbureau VNK, 2015]. Eighty percent of these boils arose on Holocene channel belts [Taal, 2015]. Other dike failures in the Netherlands attributed to piping occured in Nieuwkuijk in 1880 and Tholen in 1894 [Vrijling et al., 2010]. The danger of piping is recognized in other countries as well. A dike failed as a result of piping in New Orleans during hurricane Katrina. The breach occured a few hours after the water level increased [Vrijling et al., 2010]. In addition, in Hungary piping is regularly causing (potential) dike failures. The subsurface architecture in Hungary is considered as vulnerable to piping: a layer of fine sand on top of a 300 meters thick layer of highly permeable gravel [Vrijling et al., 2010]. Dike breaches occur regularly as a result of the financial constraints on applying appropriate preventative measures.

Figure 1.3 Two observed boils near a dike, with sand eroded from the aquifer towards the surface [https://beeldbank.rws.nl, Rijkswaterstaat].

1.3 Calculating piping

The Dutch government has adopted a method to calculate piping for testing and designing dikes. This paragraph explains the formulas used for this method. The definitions of the parameters used in the formulas are listed in Table 1.1. During the first phase, the water level in the river (ϕ_0) rises, resulting in an increased hydraulic head (ϕ_2) at the inner toe of the dike. This location has the smallest distance from the river and therefore the highest hydraulic head. Equation 1.1 is the prescribed formula to calculate the hydraulic head at the inner toe of the dike [TAW, 1985]. Figure 1.1 shows the parameters that are used for this formula in a cross-section. The second phase occurs when the hydraulic head exceeds the critical hydraulic head ($\phi_2 \geq \phi_{z,g}$). Equation 1.2 is the prescribed formula to calculate the critical hydraulic head [Föster et al., 2012]. It assumes that after the cohesive top layer has breached, the hydraulic head cannot exceed the critical hydraulic head because water is able to flow towards the surface.

Equation 1.1 Formula to calculate the hydraulic head at the toe of the dike [TAW, 1985].

$$\phi_2 = \phi_3 + (\phi_0 - \phi_3)\frac{\lambda_3}{\lambda_1 + L_2 + \lambda_3}$$

$$\lambda = \sqrt{kDc} \qquad c = d/k_v$$

Equation 1.2 Formula to calculate bursting of the top layer, including 0,3d reduction [Föster et al., 2012].

$$\phi_{crit} = h_p + d\frac{\gamma_{nat} - \gamma_w}{\gamma_w} + 0{,}3d$$

The third phase is calculated with the recently improved formula of Sellmeijer [2011], which is shown in Equation 1.3. It assumes a standard dike, built on a homogeneous sand body and horizontal layer boundaries [Knoeff et al., 2009 and Förster et al., 2012]. It can either calculate the required seepage length (L) or the critical hydraulic head (ΔHc). For this research, the required seepage length is considered as output of the model and ΔHc as input. The unit of the critical hydraulic head is in meters and is calculated by subtracting the hydraulic head from the critical hydraulic head (ϕ_{crit}-h_p). Piping is expected to occur when the available seepage length is smaller than the required seepage length.

Equation 1.3 The improved Sellmeijer formula [Sellmeijer, 2011].

$$\frac{\Delta Hc}{L} = F_{resistance} * F_{scale} * F_{geometry}$$

$$Fresistance = \frac{\gamma'_p}{\gamma_w}\{\eta \tan(\theta)\}\left(\frac{RD}{RD_m}\right)^{0,35}$$

$$Fscale = \frac{d_{70m}}{\sqrt[3]{\kappa L}}\left(\frac{d_{70}}{d_{70m}}\right)^{0,4}$$

$$Fgeometry \overset{MSeep}{=} F(G) \overset{standarddike}{=} 0{,}91 \cdot \left(\frac{D}{L}\right)\frac{0{,}28}{\left(\frac{D}{L}\right)^{2,8} - 1} + 0{,}0$$

Table 1.1 Parameters used in the formulas to calculate piping.

symbol	parameter	unit
ϕ	hydraulic head	[m+NAP]
λ	seepage factor	[m]
k	permeability of the aquifer	[m/d]
c	hydraulic resistance of the top layer	[d]
d	thickness of the top layer	[m]
k_v	vertical permeability of the top layer	[m/d]
ϕ_{crit}	critical hydraulic head	[m+NAP]
h_{zand}	head of top of permeable layer	[m+NAP]
h_{mv}	surface head	[m+NAP]
h_p	(ground) water level in hinterland	[m+NAP]
γ_w	unit weight of water	[kN/m^3]
γ_{dr}	unit weight of dry soil	[kN/m^3]
γ_{nat}	unit weight of wet soil	[kN/m^3]
H_c	critical hydraulic head	[m]
γ'_p	unit weight of particles	[kN/m^3]
γ_w	unit weight of water	[kN/m^3]
θ	rolling angle	[°]
η	White coefficient	[-]
κ	intrinsic permeability	[k μ/γ_w]
d_{70}	70% value of a grain size distribution	[m]
d_{70m}	average d_{70} in small-scale tests	(2,08 E-4 m)
D	thickness of the aquifer	[m]
L	seepage length	[m]
RD	relative density	[-]
RD_m	average RD in small-scale tests	(0,725)

1.4 Problem definition

The method to calculate piping is a steady-state 2D approach. The parameters used in the formulas are limited to one characteristic value and without time dependency. Choosing the correct value for each parameter is difficult for datasets with a wide distribution. Engineers are forced to choose safe values to deal with this wide distribution and uncertainties in the parameters. This results in the construction of (unnecessary) expensive dikes. In the Rhine-Meuse delta, many dikes are built on top of heterogeneous deposits of meandering rivers. The following parameters contain large variations in deposits of meandering channel belts: permeability (k), thickness of the top layer (d), thickness of the aquifer (D), grain size (μm). The Sellmeijer formula is recently improved by practicing many small-, medium- and large-scale experiments [Knoeff et al., 2009; Sellmeijer et al., 2011; Förster et al., 2012]. The new model fits more accurate with the results from the experiments for homogeneous fine

sediment (d_{70} = 180 µm) and less accurate with coarser sand (d_{70} = 250 µm) with a difference of 25% between measurements and predictions. ARCADIS [2012] has done an explorative study on the effects of the new Sellmeijer formula of almost 700 km of dike. The outcome was that the new Sellmeijer formula calculates up to two times more required seepage length compared to the old formula [Sellmeijer, 1989]. Koopmans and Van den Berg [2015] have studied small-scale variability in grain size, permeability and top layer thickness of a fossil channel belt in the center of the Rhine-Meuse delta. The variation in the data (d_{70} and layer thickness) of this study is large: choosing the right input value to give a realistic result is hard. Using safe values for grain size and layer thickness in the calculations will give extraordinary large required seepage lengths. Geological knowledge, such as sand-depth maps [Cohen et al., 2009], are considered a good first predictor for the risk of piping.

The limitation of the prescribed method to calculate piping is its two-dimensional approach for the first phase (groundwater flow) and the third phase (backwards erosion). It results in large uncertainties in required seepage lengths. In addition, the improved Sellmeijer formula results in larger required seepage lengths. The risk for piping is hard to determine for complex subsurfaces with large variations in grain size and layer thickness because the formulas do not consider these three-dimensional variations. The need for a new or modified method to calculate the piping process is high.

1.5 Research aim and research question

The aim of this research was investigating the behavior of ground water flow in heterogeneous subsurfaces (first phase) by using a three-dimensional groundwater model (iMOD) and visualize the risk for breaching of the top layer during a flood wave (second phase). The results are compared with the results of the prescribed method for calculating piping. This thesis is a pilot study for further research. Therefore, the formulation of new hypotheses is important and an aim in this research.

The following research question is formulated:
What are the advantages and challenges of using a three-dimensional model for calculating groundwater flow underneath dikes in heterogeneous subsurfaces, and how does this relate to the current method? It is postulated that such a model is necessary for a proper understanding of the behavior of piping.

1.6 Approach

In order to address the aim of this research, a three-dimensional groundwater model named iMOD [Vermeulen and Minnema, 2014] is used to investigate the hydraulic head induced by an arriving flood wave in a subsurface with simple and complex heterogeneity. The subsurface schematization is based on borehole descriptions and core penetration tests, which are collected for an explorative study to heterogeneity of meandering and braiding river deposits [Koopmans and Van den berg, 2015]. Geological knowledge about these different deposits is used to supplement the knowledge from the field data. Schematizations with simple variations consider a straight homogeneous sand body with varying dimensions and orientations, deposited on top of a thick permeable sand body. Complex schematizations consider a channel belt with shapes and dimensions based on the channel belt occurring in the research area. A distinction is made in permeability for different lithological units within the channel belt. This is a first step in modeling heterogeneity for groundwater flow underneath dikes. The hydraulic head, which is output of the calculations with iMOD, is compared with critical hydraulic head for bursting of the top layer. The number of days the hydraulic head exceeds the critical hydraulic head is set as a measure for the risk of piping. This measure is used to investigate the advantages and challenges of three-dimensional groundwater modeling. The results are compared with the results of the traditional method for calculating piping.

2 Geological and physical description of the study area substrate

2.1 Study area and available data

The study area is located in the central part of the Rhine-Meuse delta, north of the river Waal and close to the village IJzendoorn. Figure 2.1 shows the primary dikes along the river and marks the research area within the dashed circle. A small lake is present at the riverside of the dike, created by sand mining. During a flood wave, water will enter the aquifer from this lake and the river. At three locations, the dike has failed in the past at the exact location of the channel belt. Three small pools are located at the inner side of the dike, which are formed by dike breaches (Figure 2.1). It is not proved that piping caused these dike failures, but it confirms the potential risk of fossil channel belts close to the surface.

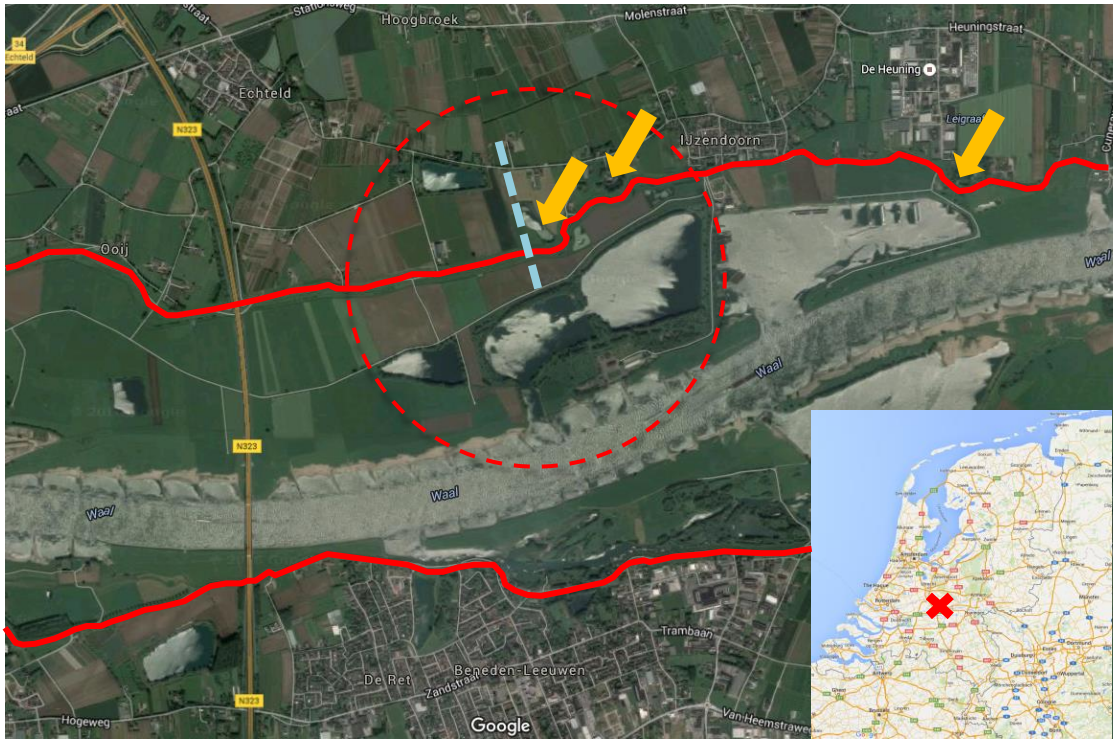

Figure 2.1 An overview of the research area. Previous research is carried out within the area indicated by red dashed circle [Koopmans and Van den Berg, 2015]. Red lines are the primary dikes, orange arrow are the locations of dike failures from the past. The dashed blue line shows the location of the lithological cross section.

In this research area, a study to specify the natural variations in different parameters that the Sellmeijer formula uses was carried out by Koopmans and Van den Berg [2015] to collect a large amount of data. In total 256 boreholes are performed in a square area of 75x75 m with a distance of five meter between the boreholes and to a depth of four meter. The collected parameters are layer thickness, lithological unit, estimation of grain size and surface elevation (Table 2.1). More than 300 sieve tests are performed to determine the grain size. Fourty core penetration tests (CPT) are performed to a depth of ten or thirty meters. Thirty CPTs are

performed in the toes on the inside and outside of the dike. Ten CPTs are performed perpendicular on the channel belt. One mechanical drilling is accomplished to a depth of 37 meters to perform three pumping tests to determine the permeability of the aquifers (Appendix I). The presence of a channel belt results in large local variations layer thickness and grain size. The channel belt deposits are hydraulically connected to the active river and the underlying Pleistocene deposits. Such hydraulic connections allow groundwater exchange. Figure 2.2 shows a lithological cross-section from the channel belt, created with the data from the borehole descriptions and CPTs [Taal, 2015]. The architecture of the channel belt contains large variations in layer thickness and grain size (coarse sand is red, fine sand is yellow). Channel fillings are marked by the red circles. The red arrow marks the location of the incision. The top layer (green) varies between 0.5 and 3 meter in this cross-section.

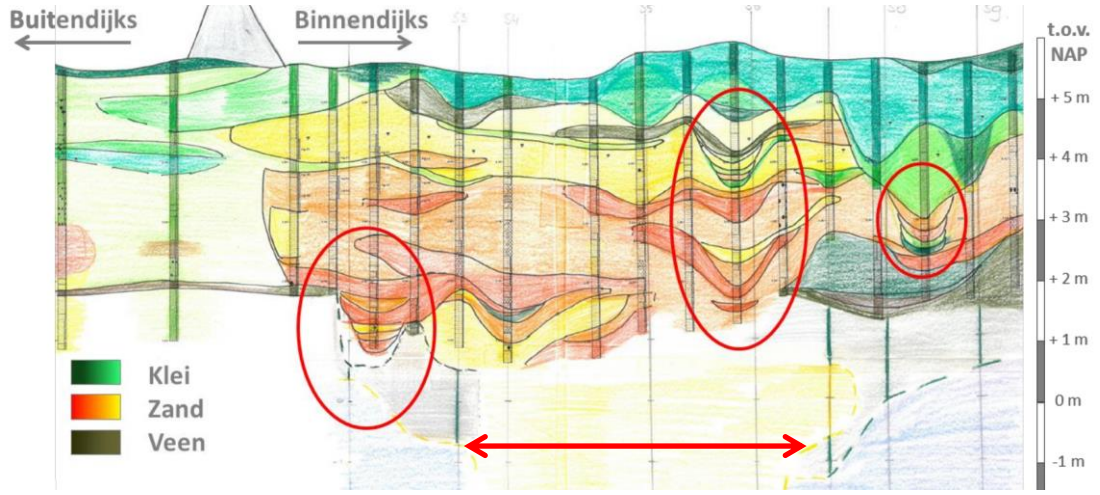

Figure 2.2 Lithological cross section of the channel belt in the research area [Taal,2015].The location of this profile is given in Figure 2.1.

Table 2.1 summarizes the data that is collected by this previous research in the study area. It shows the data from the pumping tests, borehole descriptions and sieve tests. More data is collected (CPTs and borehole descriptions), which can be found in Slot and Hertogh (2015).

Table 2.1 Summary of the dataset collected by Slot and Hertogh, [2015].

parameter	n	min value	max value	average value
grain size, d_{70} (µm)	256	162	728	420
top layer thickness channel belt (m)	256	0.2	2.4	1.4
surface head (m+NAP)	256	5.3	5.7	5.5
permeability channel belt (m/d)	1	10	10	10
permeability Pleistocene aquifer (m/d)	9	16	105	59

2.2 Properties of braided river and meandering river deposits relevant to piping

River deposits dominate the substrate in the Rhine-Meuse delta in the Netherlands. At two to ten meters depth, a thick layer of dominantly sand and gravel is present that is deposited during the Late Pleistocene by braided rivers. It is overlain by more heterogeneous deposits from meandering rivers and floodplains. These buried the deeper formations as the sea head rose. In the central and lower parts of Rhine-Meuse delta, this resulted in the following typical physical setting: large areas with clay and peat between channel belts on top of older deposits from the Late Pleistocene. Figure 2.3 shows the fossil channel belts in the Rhine-Meuse delta, which are formed during the Holocene. The physical setting differs along the rims of the delta, at the upstream end, and in the IJssel valley to the northeast of the main delta. In the latter area, aeolian deposits are of relevance as the substrate is present immediately below the dike. These are uniform and in that substrate, the restrictions of the current calculation methods for piping are less problematic. Therefore, the focus in this study is on the more heterogeneous deposits of river systems underlying the dikes.

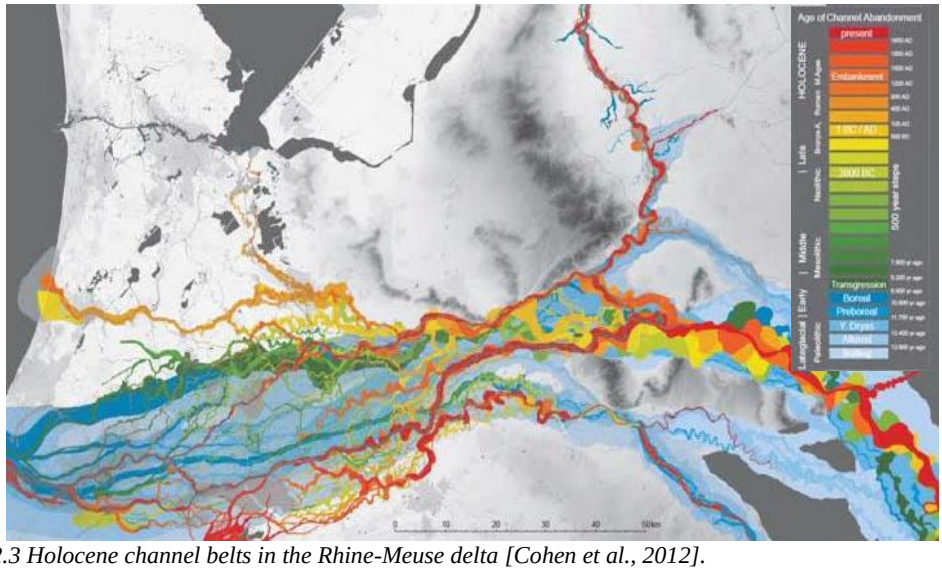

Figure 2.3 Holocene channel belts in the Rhine-Meuse delta [Cohen et al., 2012].

The data shows that the deposits of the braided river system are 30 meters thick and 7 meter below the surface [Slot and Hertogh, 2015]. At 35-40 meters depth the Formation of Sterksel is present[Westerhoff, 2003]. This formation is considered as the bottom boundary for the schematizations in this research. Directly below it, a widespread clay layer isolates deeper aquifers. Therefore, only the first aquifer influences the direct groundwater flow underneath dikes. Holocene deposits cover the permeable Pleistocene layer, containing layers of permeable and impermeable materials. This paragraph explains the hydraulic difference in permeability and conductive properties between braided and meandering river deposits. The

properties of the Pleistocene sand body mainly effects on the first phase of piping, where a head-gradient induced groundwater flow through this layer towards the polder is considered.

During the Weichselien (115.000 – 11.700 years ago), the mean sea head was up to 110 meters lower than the present situation [Berendsen, 2008]. The main rivers in the Netherlands were flowing through a valley that became the Rhine-Meuse delta during the Holocene. The slope of the river was relatively large because there was no influence from the sea, the weather conditions were cold and vegetation was sparse [Berendsen, 2008]. The resulting river style was that of braiding rivers. The river system deposited sand and gravel layers (the Kreftenheye formation) that are 0.5 meter below the surface in the East of the Netherlands and 15 meter below the surface in the West. Typical grain sizes of sand and gravel of this formation are respectively 210 - 2000 μm and 5.6 - 63 mm [Busschers and Weerts, 2003]. The top part of the Kreftenheye Formation contains finer grained sediment than the layers below. Deposits of braided river systems are dominated by sand and gravel, and generally contain very little mud and silt [Prothero and Schwab, 1996]. This means low variability between horizontal and vertical permeability. In addition, the permeability of these deposits is relatively high compared to other types of river systems. The accretion of subunits in the deposits (bar lobes and channel fills) is generally vertical, lateral accretion is less common [Gibling, 2006]. The internal architecture depends on the location in the river. Longitudinal bars divide the river in multiple channels, aggrade downstream and are formed during high-flow-velocity conditions [Prothero and Schwab, 1996]. Cross-bedded sets in sand and gravel are frequent and show avalanche stratification (Figure 2.4). Fining upward sequences are formed as the bars migrate downstream [Lunt et al., 2004]. The grain size decreases towards the surface as the bar-head migrates over the bar-tail. Longitudinal bars can become islands if vegetation is able to grow on top of these bars. In the Rhine-Meuse delta this did only occur at the end of the Weichselien because the temperature was generally too low. Transverse bars are generally formed at the side of the river. These bars are formed during low-flow-velocity conditions and aggrade perpendicular to the flow direction [Prothero and Schwab, 1996]. Figure 2.4 shows the deposition patterns of longitudinal bars and transverse bars. The top of the Wijchen member (clay and silt) covers the braided river deposits with a thickness of 0.5 – 1.0 meter [Berendsen 2008]. The Wijchen member forms the boundary between Pleistocene and Holocene deposits. The layer is not always present because of incision of younger river systems.

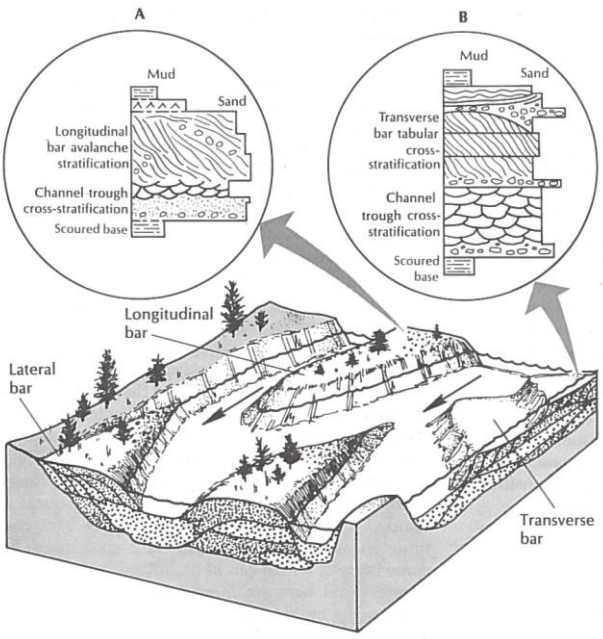

Figure 2.4 The internal architecture of a longitudinal bar and a transverse bar [Prothero and Schwab, 1996].

The Holocene deposits are relevant to all three phases in the piping process. Permeable deposits, allow groundwater exchange from deeper deposits or from the river into the channel belt. The channel belt is covered by a top layer of clay, which is formed by suspended load, settled in the wake of high water events. The thickness of this confining top layer influences the second phase of the piping process. The top of the sand layer directly beneath the top layer is eroded during the final phase of piping. Grain size distribution is therefore an important variable for the final phase. At the beginning of the Holocene 11.700 years ago, the Rhine-Meuse river system transferred from a braiding system into a meandering system [Berendsen, 2008]. This change in fluvial style is caused by the combination of sea level rise that decreased the slope of the river and vegetation growth [Berendsen, 2008]. Meandering river deposits contain a wide range in grain size [Koopmans and Van den Berg, 2015; Prothero and Schwab, 1996]. Figure 2.5 shows a schematic cross section of a meandering river. Different lithological units are showed in the figure. Permeable deposits within the channel belt are the most relevant for piping. The properties of these deposits are discussed below.

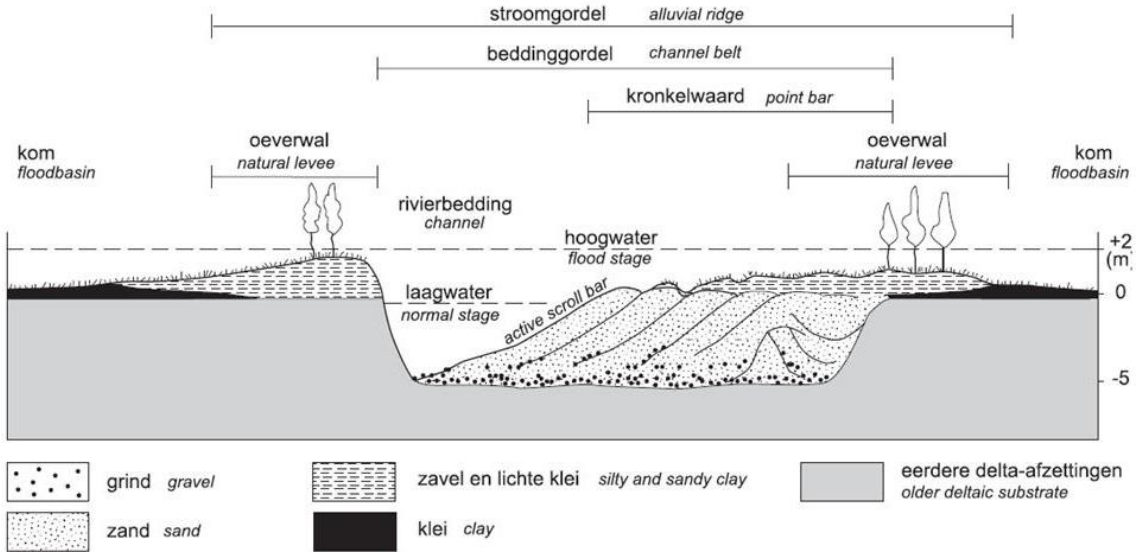

Figure 2.5 The complex architecture of a meandering river, large variations in grain size are found within the channel belt [Cohen et al. 2009].

Channel lag deposits form the basal bottom boundary of a meandering channel belt. Bed load (coarse sand and gravel) is transported during high discharges and will not leave the channel [Prothero and Schwab, 1996; Berendsen, 2008]. This layer of course sediment has a high permeability. It can be recognized during the field research by its sharp boundary between other lithological units. Spatial variations in permeability of bed forms on a small scale have large influence on groundwater flow [Bridge, 2003]. Meandering river channels incise older deposits. If the older deposits consist of sand layers, access for ground water is created to flow from older sandy deposits into the channel belt. The risk for piping becomes larger because the thickness of the aquifer becomes significantly larger, resulting in a higher hydraulic head [Sellmeijer, 2006]. Point bars are located at the inner bend of a meander and are characteristic for this fluvial style. Point bars are deposited on top of older channel lag deposits (Figure 2.6) with vertical and lateral accretion [Berendsen, 2008; Prothero and Schwab, 1996 and Gibling, 2006]. The deposited material on top of point bars is finer, with an increasing grain size towards the base of the point bar [Miall, 1996]. The deposition pattern is diagonal, which is recognizable by reactivation surfaces that contain clay or silt, which is deposited when high water decreases to normal water level.

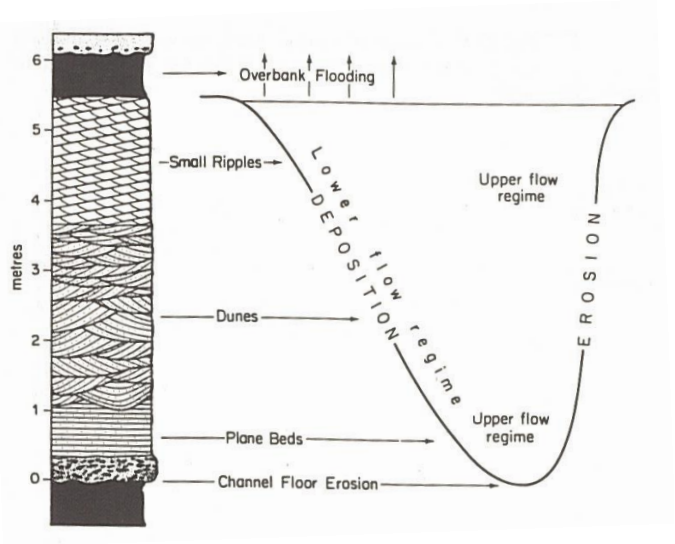

Figure 2.6 Example of a point bar, which is deposited on top of a channel floor [Miall, 1996].

Toonen et al. [2012] investigated different abandoned river channel fills. Such fills result in variations in top layer thickness. The resulting avulsion-splay complexes contain almost all clastic units, depending on the distance from the bifurcation [Berendsen, 2008]. In general, the filling contains fine sediment [Bridge, 2003]. The filling of the channel is longitudinally and vertically sorted. Close to the bifurcation, thick layers of sand are deposited, while the grain size and the layer thickness become smaller as the distance from the bifurcation increases [Toonen et al., 2012].

Natural levees are located at the inner and outer bend of a meandering river. The material is generally fine sand at the base of the levee, and becomes finer as the levee increases in height (fining upward) because coarse material cannot overtop the levee as it increases in height [Berendsen, 2008]. The preservation of the deposited material depends on many factors: the distance between an active river and the fossil channel belt, the timescale and the stage of the river [Lewin and Macklin, 2003]. During an incising stage, the river erodes vertically into older deposits. The river erodes horizontally during aggrading stage, with more preservation of sediment. Figure 2.7 shows the development of the Allier. The deposited material within the channel belt is not preserved entirely. Figure 2.8 shows the horizontal and lateral migration of a meandering river in a cross section. The result of this dynamic behavior is large variations in grain size and layer properties.

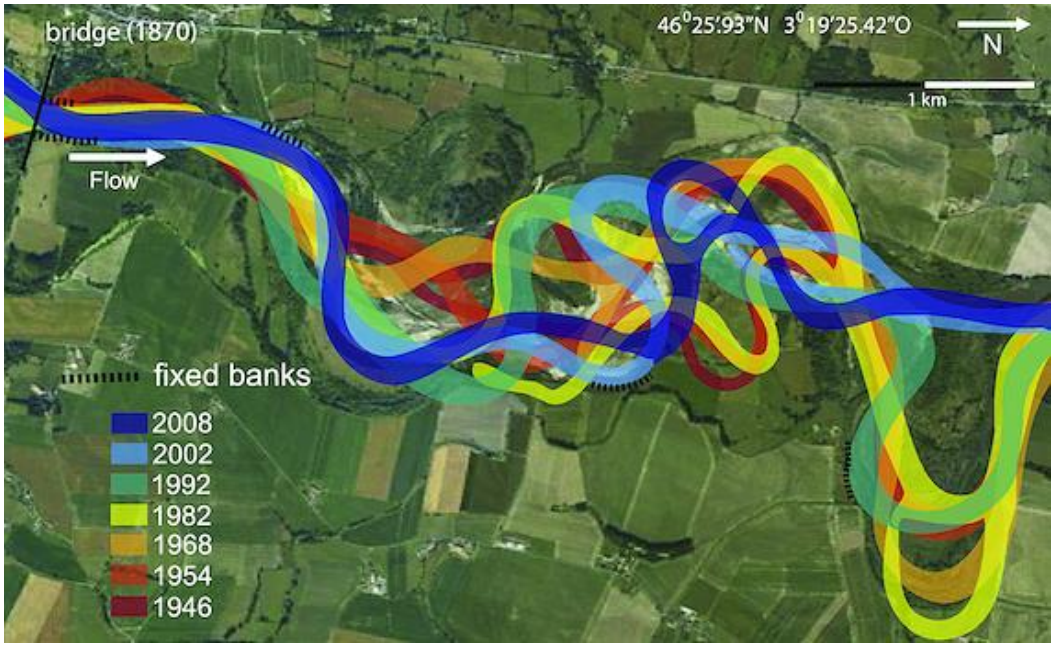

Figure 2.7 The development of a meandering river in 58 years [Van Dijk et al., 2012].

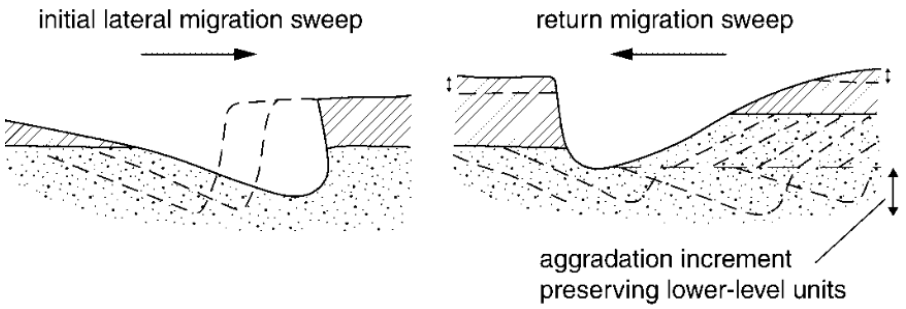

Figure 2.8 Horizontal and lateral migration of a meandering river [Lewin and Macklin, 2003].

3 Methods and model settings

3.1 Introduction to iMOD

The software package iMOD (interactive modeling) is used to model the subsurface and calculating groundwater flow [Vermeulen and Minnema, 2015]. iMOD is designed to visualize and analyze three-dimensional subsurface data. In addition, it contains the MODFLOW calculation engine for executing groundwater calculations. This makes it a tool for calculating the first phase of the piping process with a three-dimensional schematization of the subsurface. The calculations for groundwater flow are based on Darcy's law (Equation 3.1) and volumetric budget. The volumetric budget is based on the incoming and outgoing groundwater in the model. Groundwater flow is calculated with a finite difference approach and uses a block grid for multiple subsurface layers. The Input Data File (IDF) contains the necessary input data for each parameter to run the model. An IDF is a raster file and contains a parameter-value for each raster point. iMOD is able to run either steady-state or transient calculations. A flood wave is simulated by transient calculations with a varying water level in the river for each time step. A more detailed description of the calculation methods in iMOD and MODLOW is given by Harbaugh [2005] and Vermeulen and Minnema [2015].

Equation 3.1 Basic formulation Darcy's law [Harbaugh, 2005].

$$Q = \frac{KA(h_1 - h_2)}{L}$$

Where

Q	volumetric flow	[m^3/s]
K	hydraulic conductivity of the material in the direction of flow	[m/s]
A	cross-sectional area perpendicular to the flow	[m^2]
$h_1 - h_2$	head difference across the prism parallel to flow	[m]
L	length of the prism parallel to the flow path	[m]

The river-package (RIV) in iMOD is developed to simulate a river [Vermeulen and Minnema, 2015]. The RIV-package allows a higher water level than the surface elevation, assuming that water only will enter the aquifer. The RIV-package contains four parameters: conductance, bottom elevation, water level and infiltration.

- Conductance (m^2/d) of the river represents the discharge of water that seeps from the river into the aquifer. The amount of mud and clay on the riverbed influences the river conductance. More resistance caused by this less permeable material results in a lower conductance and therefore less water seeping into the aquifer.
- iMOD uses the bottom elevation (m+NAP) to determine which aquifers are connected with the river.

- iMOD assumes an unlimited capacity of water in the river [Vermeulen and Minnema, 2015]. This means that water level (m+NAP) will be a consistent value, given by the user for each time step.
- The infiltration factor (-) is a measure for water that infiltrates from the aquifer towards the river as the hydraulic head is larger than the river level.

3.2 Modeling process

Figure 3.1 shows a flow chart of the modeling process. The green blocks represent different input parameters that are used to schematize the subsurface, boundary conditions and calculation settings. This information is input for iMOD (blue blocks). The parameters that contain local variations are stored in IDFs (Appendix III), for example permeability contains variations within each model layer. Parameters without local variations are either stored in IDFs or used as fixed value in the RUN-file to save data storage (Appendix II). The RUN-file describes the calculation settings and refers to the input data. iMOD reads the RUN-file and executes the calculation. The output of the transient calculations is an IDF with the hydraulic head for each time step and each layer. iMOD does not take bursting of the top layer into account (phase 2 of the piping process). Therefore, the hydraulic head can exceed the critical hydraulic head for breaching of the top layer. The output data used for this research is the hydraulic head, which is calculated for each time step. The results are exported to Matlab (Appendix IV). Scripts are created to import, store and analyze the data. Figures are created to investigate the behavior of the hydraulic head and to compare the hydraulic head with the critical hydraulic head. Finally, the results of the Sellmeijer formula are compared with the results of iMOD (Appendix V).

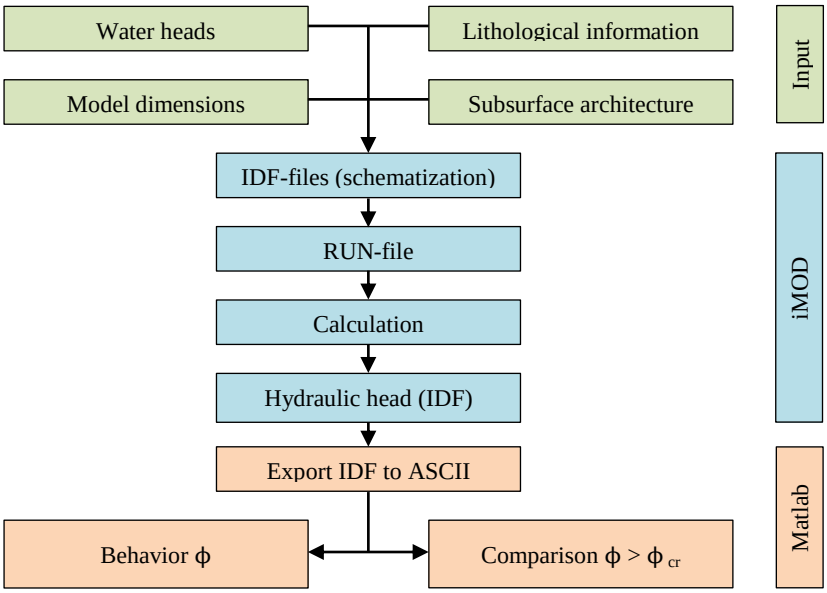

Figure 3.1 Flow chart of the modeling process.

3.3 Schematization of different scenarios

Two different schematizations of the subsurface are created in iMOD. The first schematization contains simple three-dimensional variations. The second schematization contains complex three-dimensional variations in lithological units within the channel belt. Both schematizations contain an aquifer with a thickness of 30 meters that represents the Pleistocene deposits. The simple schematization contains a straight channel belt on top of the Pleistocene deposits. This results in varying top layer thicknesses because the channel belt is deposited closer to the surface. In addition, the permeability varies between the Holocene and Pleistocene deposits. Different scenarios are modeled to investigate the influence of the orientation, width and incision width of the channel belt. Table 3.1 summarize the values that are used for each investigated scenario. Figure 3.2 shows the investigated scenarios of the simple schematization.

Table 3.1 Values used for each scenario with a simple schematization of the subsurface.

scenario	width	incision width	orientation
orientation of the channel belt	700 m	700 m	45 and 90°
width of the channel belt	20, 40, 60, 80, 100, 200, 300, 400, 500, 600 and 700 m	equal to the width	90°
incision width of the channel belt	700 m	0, 20, 40, 60, 80, 100, 200, 300, 400, 500 and 600 m	90°

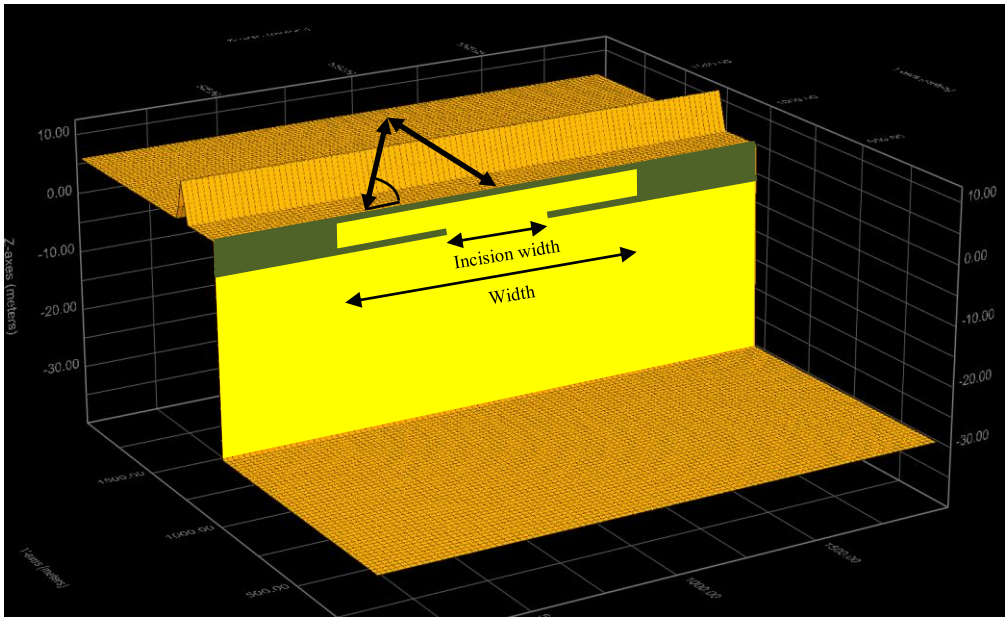

Figure 3.2 Cross-sectional description how a partly incised channel belt is modelled (yellow = aquifer, green = aquitard). The arrows indicate the orientation of the channel belt which are investigated.

The complex schematization is modeled for a larger area with a higher resolution. This was necessary to implement small variations. The channel belt is created with five layers with a thickness of one meter (Figure 3.3). Each layer represents a different lithological unit, based on architecture of meandering river deposits (Figure 2.5). The dimensions and shape of the channel belt are based on sand depth maps (Figure 2.3). The schematization contains coarse material at the bottom of the channel belt. The sediment becomes finer as it gets closer to the surface. The top of the channel belt is one meter below the surface and represents natural levees and a residual channel filled with clay.

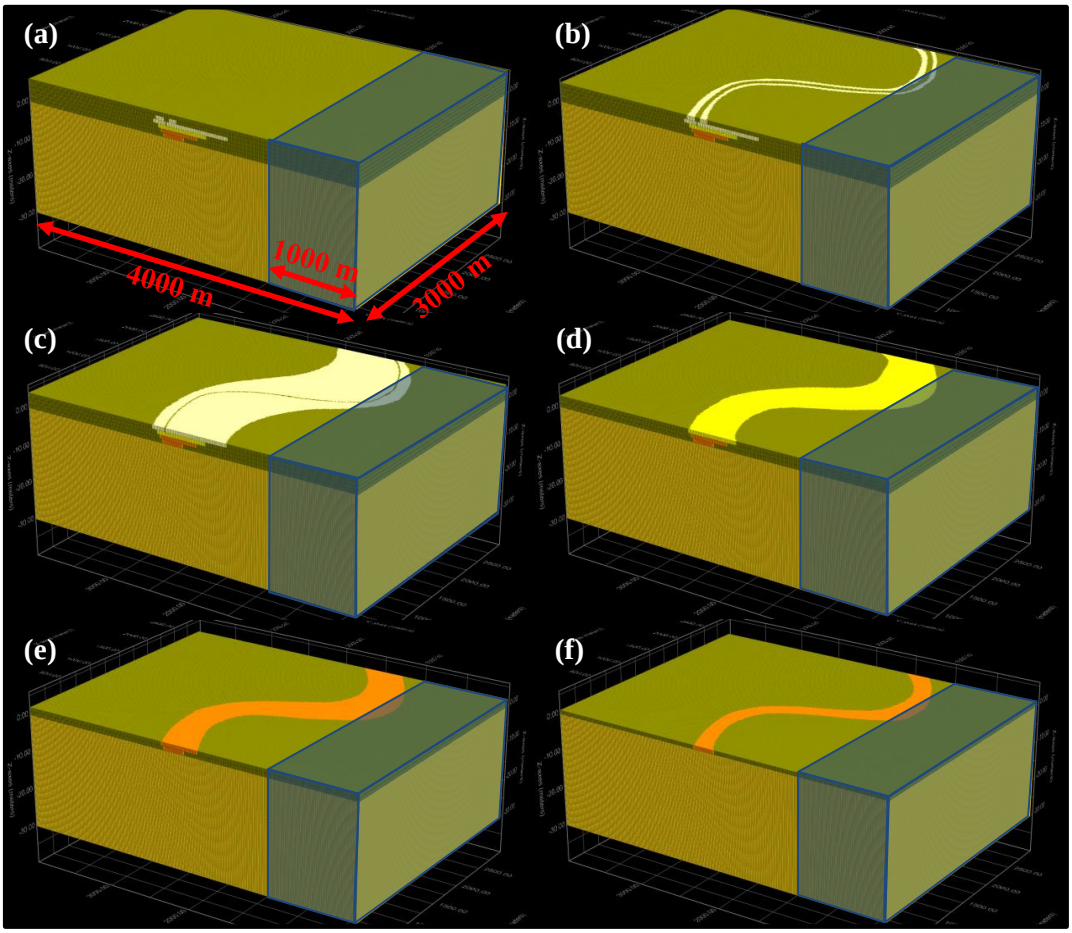

Figure 3.3 Schematization of the Holocene channel belt on top of thick sand body from the Pleistocene era. Green is clay, yellow is sand and orange is gravel. The location of the river is indicated by the shapes, which are in contact with the channel belt. Each layer of the Holocene channel belt is one meter thick. (a) top layer of clay. (b) Natural levees of fine sand with a low permeability and channel fill deposits of clay. (c) Fine sand, spread over a large width including a small residual channel. (d) Coarse sand with a permeability of 10 m/d. (e and f) Channel lag deposits of gravel with a high permeability of 105 m/d, in contact with the thick sand body below.

Three scenarios are investigated with this complex schematization: (1) a channel belt connected with the river, (2) a channel belt incises the Pleistocene sand body and (3) the combination of both hydraulic connections. Figure 3.3f shows the hydraulic connection with the Pleistocene sand body by a layer of gravel. For the scenario without incision, this connection is removed by changing this layer of gravel to clay. The hydraulic properties of all

layers of the channel belt are changed to schematize a scenario of a channel belt without hydraulic connection with river. The hydraulic connection with the river is removed by changing the aquifers that are in contact with the river to clay within a distance of 100 meters from the river.

3.4 Input parameters

The input parameters used to create the schematizations of the subsurface are explained in this paragraph. An overview of all used values is given in Table 3.2 at the end of this paragraph. The dimensions of the model, used in the simple schematization are 2.000 x 2.000 meters with a pixel size of 10 x 10 meters. The dimensions of the complex schematization are 3.000 x 4.000 meters with a pixel size of 5 x 5 meters. For all calculations, the boundary conditions at the edge of the model were set to active. This means that groundwater can exit the model at the edges, depending on the gradient of the hydraulic head. This is considered as the best option because the models are relatively small. Other options are a fixed hydraulic head and inactive boundaries. Both are limiting ground water flow at the edge of the model (edge effects), which could affect the behavior of ground water because the model is relatively small. The following assumptions simplify the model by limiting the number of variable parameters:

- the dike is absent in the schematization because it is separated from the sand body and therefore the influence on the hydraulic head is expected to be low;
- no infiltration from the river through the top layer in the floodplain because it is assumed that this layer only contains clay;
- the horizontal permeability and vertical permeability are for all lithological units identical and no anisotropy within both aquifers and aquitards are implemented in the schematization.

The maximum water level during a flood wave at the research location is a prescribed value of NAP+12.1 m [Ministerie van Verkeer en Waterstaat, 2006]. The duration is set on 21 days, based on the flood wave in 1995. Figure 3.4 shows the used flood wave in red. The flood wave starts with NAP+6 m, which is equal to the used hydraulic head in the polder. The total period used for each calculation is 32 days.

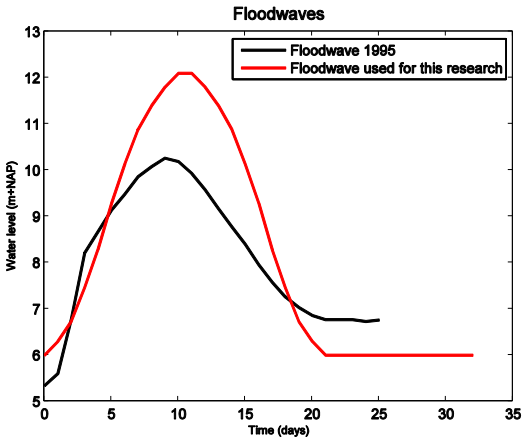

Figure 3.4 The flood wave that is modeled in all calculations and the flood wave from 1995 at the location of the research area [http://live.waterbase.nl/].

The river bottom is assumed to be at the bottom of the aquifer at a depth of NAP-30 meters. The reason for choosing this value is the small lake between the river and the dike. This lake is created by sand mining and is expected to be deep. Therefore, the vertical surface of the aquifer that is connected with the river is large, resulting in a high value for the river conductance. The distance between the river and the polder was set in the schematizations as 35 meters, although the real distance is between 150 and 250 meters. This is in line with the calculations with Sellmeijer that are executed by Koopmans and Van den Berg [2015] because this is the distance that is protected by the water board. It allows comparisons with the results of this research. The width of the dike is 65 meters, making the total available seepage length for piping 100 meters. The layer properties are based on the data from drillings and CPTs that is collected by Slot and Hertogh [2015]. According to the CPTs, the boundary between the Pleistocene sand body and the Holocene channel belt is six meters below the surface. This is visualized in the lithological cross-section (Figure 2.2). This boundary is used in all schematizations. The top layer thickness at the channel belt varies between 0.5 and 3 meters. A top layer thickness of one meter is chosen for this research. Each lithological layer is modeled with four IDFs. Two IDFs describe the top elevation and bottom elevation of each layer. Two IDFs represent the parameters of each lithological unit. These parameters are permeability (m/d) and storage coefficient (-). The storage coefficient is a measure for the amount water that can be stored in each layer. Aquifers (sand and gravel) are modeled with a relatively high permeability and a small storage coefficient. Aquitards (silt and clay) generally have a low permeability with a high storage coefficient. The permeability of the Holocene and Pleistocene deposits is based on the results from the pumping test [Slot and Hertogh, 2015]. The storage coefficients for confined layers are calculated with Equation 3.2, with typical values for each lithological unit [Domenico and Mifflin, 1965; Batu, 1998]. The storage coefficient of unconfined layers is larger than of confined layers and have a large

dependency on specific yield [Heath, 1983]. In general, the storage of unconfined layers ranges from 0.1 to 0.3 [Lohman, 1972]. The first meter of clay beneath the surface is modeled with a storage coefficient of 0.3.

Equation 3.2 Formulas to calculate storage coefficient for confined layers [Duffield, 2015].

$S = S_s\, b$

Where

S	Storage coefficient	[-]
S_s	Specific storage	[m^{-1}]
b	Layer thickness	[m]

Table 3.2 The values for each parameter used for the simple and complex schematizations of the subsurface.

parameter	**simple subsurface**	**complex subsurface**	**unit**
model dimensions	2.000 x 2.000	3.000 x 4.000	m
grid size	10 x 10	5 x 5	m
surface head	6	6	m+NAP
width of the flood plain	35	35	m
width of the dike	65	65	m
width of the river	1000	1000	m
groundwater level	6	6	m+NAP
top layer thickness (channel belt)	1	1	m
top layer thickness (without channel belt)	6	6	m
thickness of the channel belt	5	5	m
thickness Pleistocene deposits	30	30	m
bottom boundary elevation	-40	-40	m+NAP
river conductance	500	500	m^2/d
river infiltration	1	1	-
river bottom	-30	-30	m+NAP
thickness bottom layer (aquitard)	10	10	m
permeability fine sand	10	10	m/d
permeability gravel	-	105	m/d
permeability silt	-	1	m/d
permeability Pleistocene sand body	59	59	m/d
permeability clay (aquitard)	0.01	0.01	m/d
specific storage fine sand	0.00017	0.00017	m^{-1}
specific storage gravel	-	0.00008	m^{-1}
specific storage silt	-	0.00075	m^{-1}
specific storage Pleistocene sand body	0.00008	0.0008	m^{-1}
storage coefficient anthropogenic soil (1^{st} m)	0.3	0.3	m^{-1}

The risk for breaching of the top layer is calculated with the hydraulic head (output of the calculation with iMOD) and the critical hydraulic head. Therefore, the critical hydraulic head is an input parameter. The critical hydraulic head is calculated for top layer thicknesses varying between one and six meters. Table 3.3 shows the used values for different parameters and the results. Other parameters used for these calculations are density of the top layer (16 kN/m), density of water (10 kN/m) and the surface head (NAP+6 meters).

Table 3.3 Critical hydraulic head for various top layer thickness.

top layer thickness (m)	**depth of base top layer (m+NAP)**	**weight of the top layer (kN)**	**0.3d (m)**	**critical hydraulic head (m+NAP)**
1	5	16	0.3	6.9
2	4	32	0.6	7.8
3	3	48	0.9	8.7
4	2	64	1.2	9.6
5	1	80	1.5	10.5
6	0	96	1.8	11.4

The required seepage length is calculated with the formula of Sellmeijer (Equation 1.3). The values used for these calculations are summarized in Table 3.4. The values for the top layer thickness are equal to the values used in the schematization in iMOD. The smallest, average and largest values for grain size (d_{70}) are used from a dataset of more than 300 sieve tests [Slot and Hertogh, 2015].

Table 3.4 The used input values for the Sellmeijer formula.

parameter	**value**	**unit**
surface head	6	m+NAP
width flood plain	35	m
width dike	65	m
groundwater level	6	m+NAP
top layer thickness	1 and 6	m
thickness aquifer	4, 30 and 35	m
Permeability aquifer	10, 52 and 59	m/d
grain size	162, 420 and 728	µm
water level	12.1	m+NAP

4 Results

4.1 Simple schematizations

Figure 4.1b and Figure 4.1c show the influence of different channel belt orientations on the hydraulic head. It presents a top-view of the river, dike and polder. The dashed red lines are the boundaries of the channel belt with a fixed width of 700 meters. The dashed blue line indicates the river. Black lines indicate the boundaries of the dike. The figure shows the hydraulic head during the maximum water level in the river. The hydraulic head is lower at the location of the channel belt where the top layer is thin. The lowest hydraulic head is found at the center of the channel belt. The hydraulic head at the center of the channel belt decreases as the orientation angle between the river and the channel belt becomes increases from 45° to 90° (Figure 4.1a). The hydraulic head at the edges of the channel belt varies with an orientation of a 45° angle. In Figure 4.1a, the left side of the channel belt contains larger differences in hydraulic head between the edge and the center of the channel belt compared to the right side.

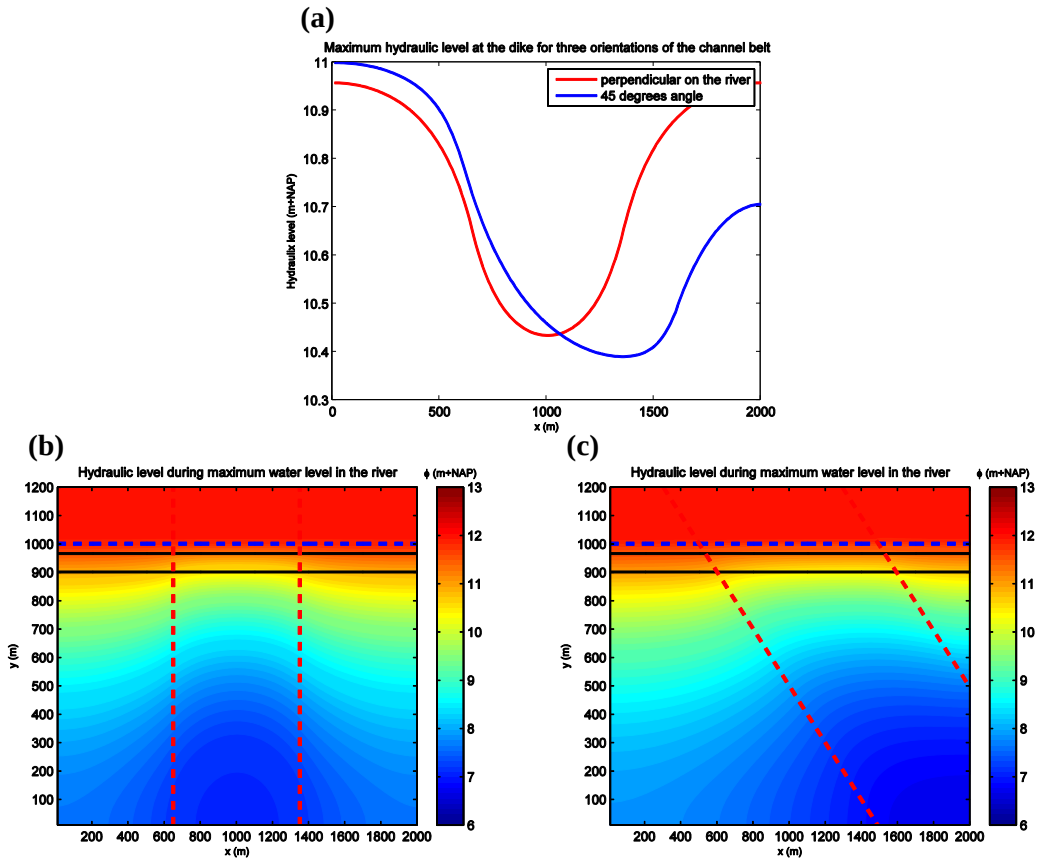

Figure 4.1 (a) Hydraulic head at the inner toe of the dike, in line the river (y = 900 meters). (b and c) Hydraulic head in the aquifer during maximum water level in the river for two channel belt orientations, Note that the x-axis and y-axis are not at the same scale.

Figure 4.2 shows the influence of varying channel belt width on the hydraulic head. Figure 4.2a shows a cross section in line with the river at the inner toe of the dike. The hydraulic head at the center of the channel belt (x = 1000 m) is relatively small compared to channel belts with a limited width. Figure 4.2b shows the relation between width of the channel belt and the difference between hydraulic head at the center of the channel belt and the polder ($\phi_{polder}/\phi_{channel\ belt}$) at the location of the dike. The difference in hydraulic head is larger for wide channel belts compared to narrow channel belts.

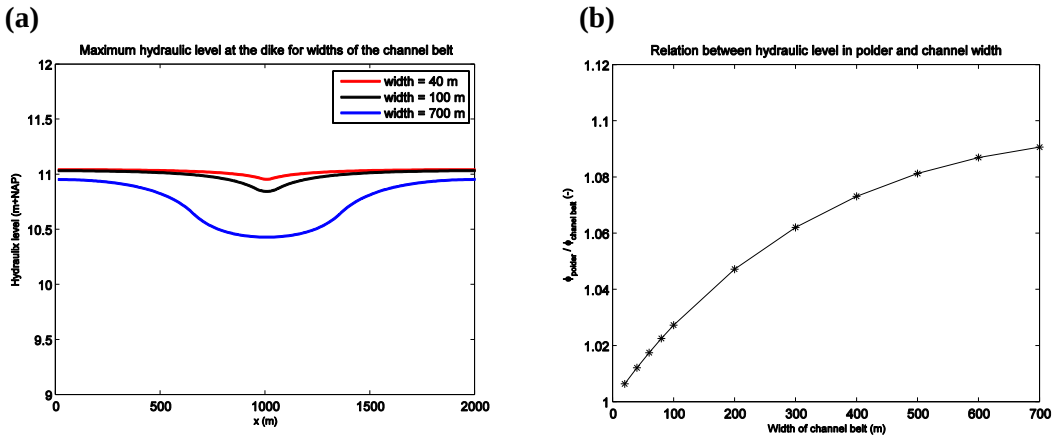

Figure 4.2 (a) Hydraulic head in line with the river at the inner toe of the dike with varying width of the channel belt. (b) Relation between width of the channel belt and the difference between hydraulic head at the center of the channel belt and the polder ($\phi_{polder}/\phi_{channel\ belt}$).

The duration of the risk for breaching of the top layer is showed Figure 4.3. The figure shows only the polder. Breaching of the top layer cannot occur in between the river and the outer toe of the dike because the weight of the top layer is much larger than the hydraulic pressure. The inner toe of the dike is present at y = 900 m. This duration is calculated with the hydraulic head and Equation 1.2. It shows the number of time steps (days) that the hydraulic head exceeds the critical hydraulic head ($\phi > \phi_{cr}$). More days with this condition means larger risks. The hydraulic head did not exceed the critical hydraulic head at the white areas. The risk for breaching of the top layer is larger for narrow channel belts. In addition, this risk extends over a larger distance away from the dike compared to a wide channel belt. For wide channel belts, the risk for breaching of the top layer decreases more significantly towards the center of the channel belt. The maximum number of days with a risk for breaching of the top layer is 16.

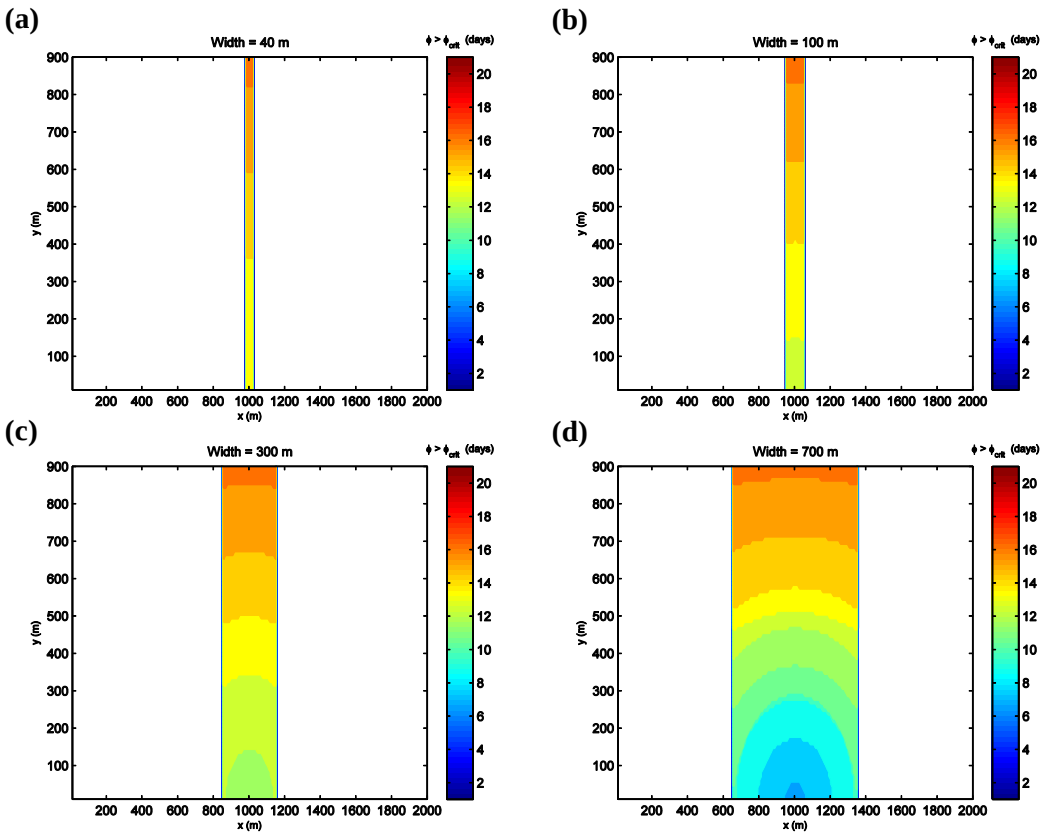

Figure 4.3 Duration of $\phi > \phi_{critical}$ for varying width of the channel belt. Only the polder is visualized in the figure, because the top layer will not breach at the location of the dike or floodplains.

Figure 4.4 shows the influence of varying incision width on the hydraulic head. Figure 4.4a compares the hydraulic head of channel belts with a large incision width (400 m) and a small incision width (40 m). The dashed lines present the hydraulic head within the channel belt (L2). The continuous lines show the hydraulic head in the Pleistocene sand body (L4). For both incision widths, the hydraulic head in both aquifers are equal at the location of the incision. The hydraulic head inside the channel belt (L2) decreases as the distance from the incision becomes larger. Figure 4.4b shows the relation between width of incision and the difference between hydraulic head at the center of the channel belt and the polder (ϕ_{polder}/ $\phi_{channel\ belt}$) at the location of the dike. The difference in hydraulic head is largest for large incision widths.

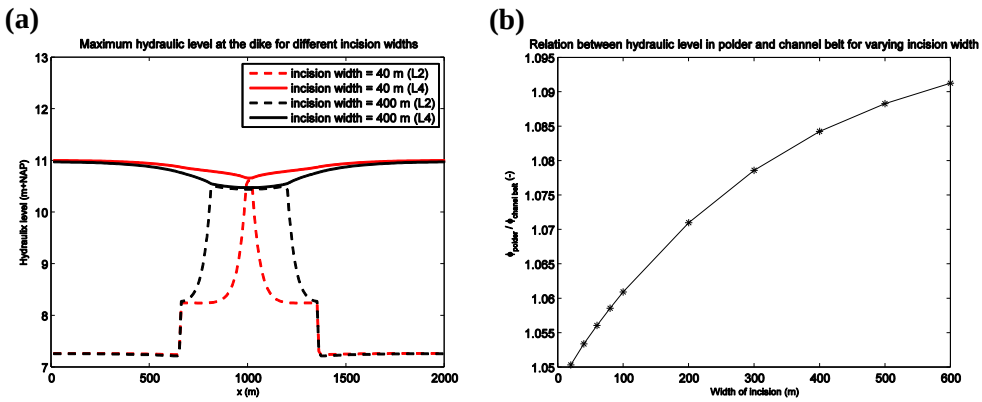

Figure 4.4 (a) Hydraulic head in the channel belt (L2) and the underlying sand body (L4) at the inner toe of the dike (y = 900 m). (b) Relation between width of incision and the difference in hydraulic head between the polder and the center of the channel belt.

The duration of the risk for breaching of the top layer with varying incision widths is showed in Figure 4.5. The hydraulic head did not exceed the critical hydraulic head at the white areas. Figure 4.5a is a situation with an isolated channel belt (incision width = 0 meter). The hydraulic head in the channel belt is induced by groundwater flow through the channel belt. Figure 4.5b, c and d show incision widths of 40, 200 and 400 meters. The risk for breaching of the top layer for all incision widths is largest at the location of the incision. The risk becomes less as the distance from the river and/or the incision becomes larger.

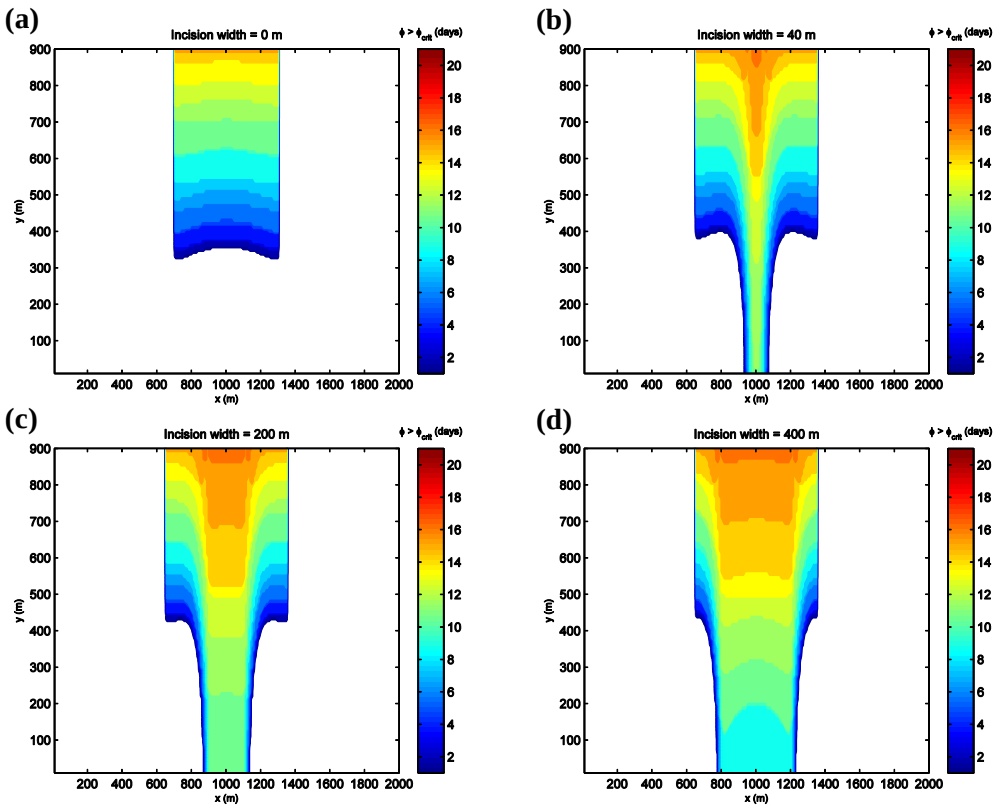

Figure 4.5 Duration of $\phi > \phi_{critical}$ for varying incision width, which varies between 0 and 400 meters. Only the polder is visualized in the figure, because the top layer will not breach at the location of the dike or floodplains.

4.2 Complex schematizations

Figure 4.6 shows the hydraulic head in the channel belt (a) and the Pleistocene sand body (b) during the maximum water level in the river. The sharp boundaries in hydraulic head within the channel belt are located at the transitions of layer properties within the channel belt. At these locations, the thickness of the channel belt and/or the top layer changes. A reduced hydraulic head in the Pleistocene sand body is present at the locations where the channel belt incises, indicated by the black arrow in the figure.

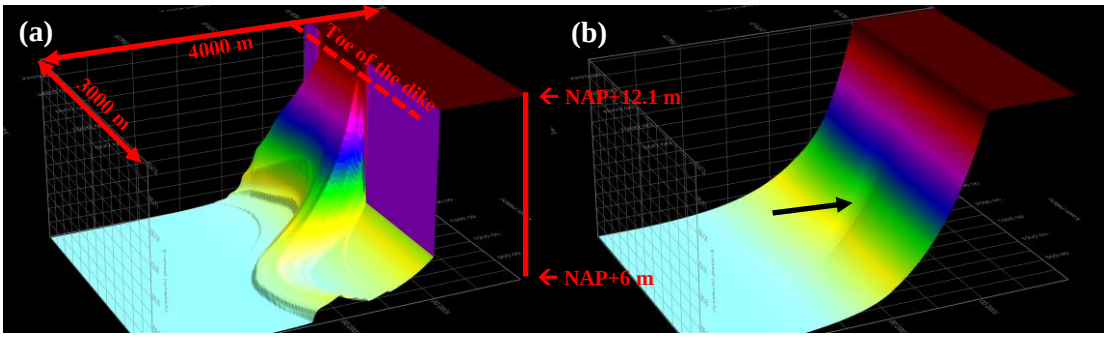

Figure 4.6 Hydraulic head during maximum water level in the river in the channel belt (a) and the underlying sand body (b).

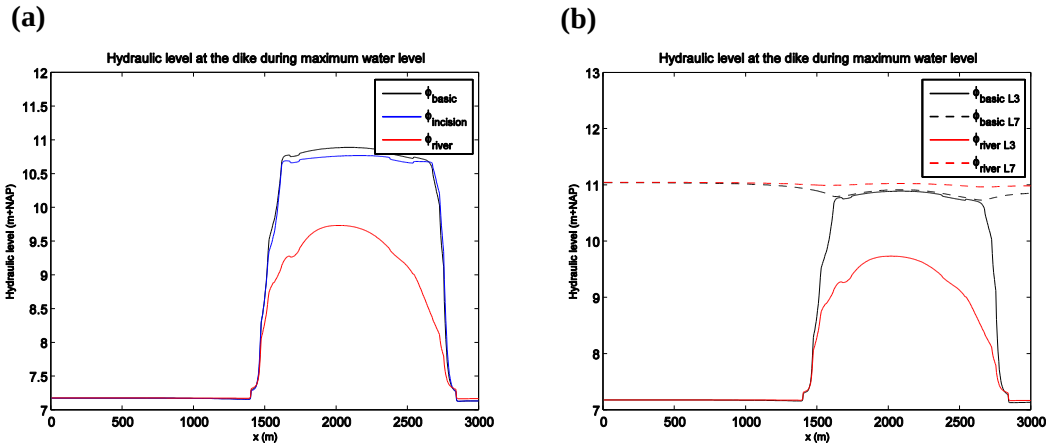

Figure 4.7 (a) Hydraulic head in the channel belt at the inner toe of the dike in line with the river, for three different situations. The channel belt is located between x = 1350 and 3000 meters. (b) Hydraulic head in the channel belt and the underlying sand body (dashed) with incision (black) and without incision (red).

Figure 4.7a compares the hydraulic head for three different hydraulic connections of the channel belt. It shows the hydraulic head located at the inner toe of the dike during the maximum water level in the river. The scenario of a channel belt that is hydraulically connected with the river and the Pleistocene sand body (ϕ_{basic}) shows the largest hydraulic head. The scenario with a channel belt incised in the Pleistocene sand body ($\phi_{incision}$) shows similar results. The hydraulic head within a channel belt that is only hydraulically connected with the river (ϕ_{river}) is lower. Figure 4.7b shows the differences in hydraulic head between

the channel belt (L3) and the Pleistocene sand body (L7) for scenarios ϕ_{basic} and ϕ_{river}. The hydraulic heads for scenario ϕ_{basic} are equal at the location of the incision between x = 1600 and 2700 meters. Scenario ϕ_{river} shows different hydraulic heads in the channel belt and Pleistocene sand body. The hydraulic head in the Pleistocene sand body is for $\phi_{river\ contact}$ larger than $\phi_{basic.}$ Figure 4.8 shows the number of days with a risk for breaching of the top layer ($\phi > \phi_{critical}$) for the three scenarios. The hydraulic head did not exceed the critical hydraulic head at the white areas. The risk is in all scenarios largest at the location of the natural levees, which are modeled as fine sand with a low permeability. Between the natural levees, a residual channel is modeled with 1-2 meters thick layer of clay. The top layer is thicker at these locations, resulting in a lower risk for breaching. The results of the scenario with only incision as hydraulic connection shows similar results are the basic scenario with hydraulic connections by incision and with the river. The risk for breaching of the top layer is lower for the scenario with a channel belt only connected with the river.

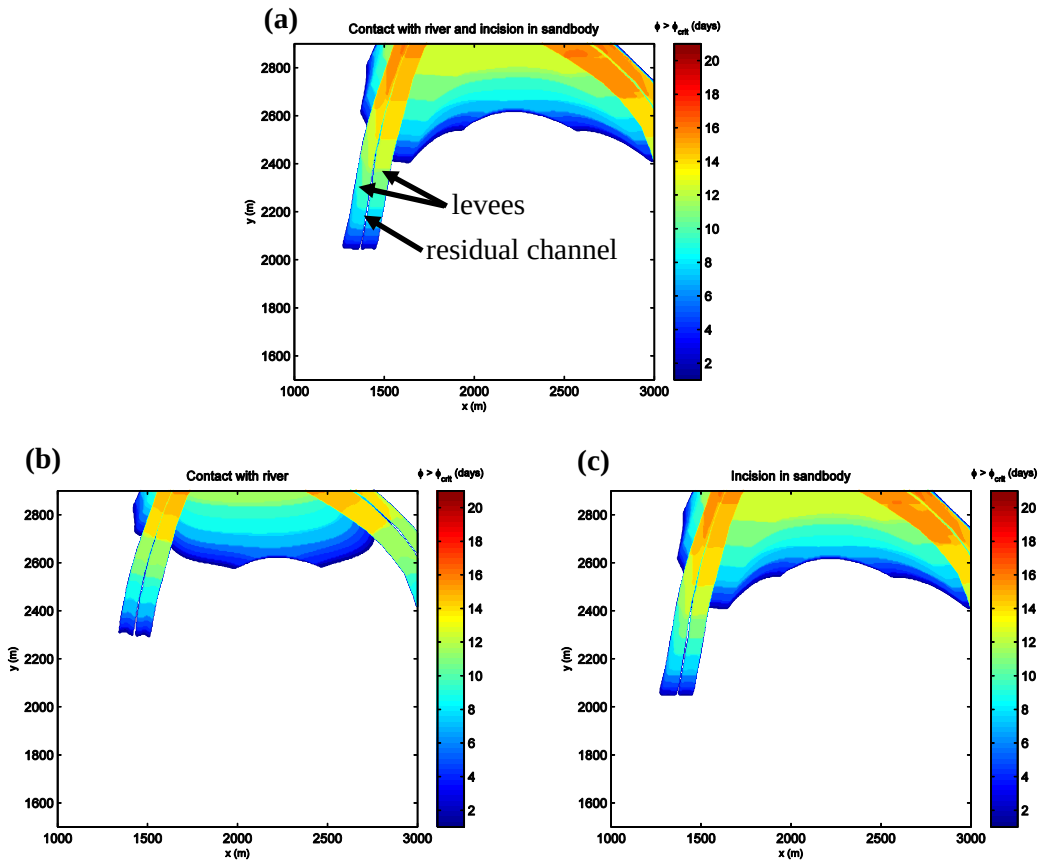

Figure 4.8 Duration of $\phi > \phi_{critical}$ for the basic situation with incision and contact with the river (a), the situation with only contact with the river (b) and the situation with only incision in the underlying sand body (c).

4.3 Sellmeijer

Table 4.1 shows the output of the Sellmeijer formula (L) for nine different input variations. Calculations 1-3 simulate a channel belt on top of an aquifer with a total thickness of 35 meters. Calculations 4-6 simulate a channel belt that is isolated from the Pleistocene sand body and only hydraulically connected with the river. Calculations 7-9 simulate a thick top layer (six meters) on top of the Pleistocene sand body. The results are only applicable for locations where the top layer is breached.

Table 4.1 Results of the Sellmeijer formula.

nr	d (m)	d_{70} (µm)	D (m)	k (m/d)	L (m)
1	1	162	35	52	**299**
2	1	420	35	52	**196**
3	1	728	35	52	**153**
4	1	162	4	10	**92**
5	1	420	4	10	**60**
6	1	728	4	10	**47**
7	6	162	30	59	**216**
8	6	420	30	59	**141**
9	6	728	30	59	**110**

5 Discussion

This research investigated the advantages and challenges of using a three-dimensional model for calculating groundwater flow underneath dikes in heterogeneous subsurfaces. This groundwater flow is the first phase in the process of piping. Simple and complex three-dimensional schematizations of the subsurface are made to investigate the behavior of the hydraulic head on three-dimensional variations in subsurface architecture. This chapter discusses the results of this research and its contribution to the understanding of piping.

The hydraulic head has a dependency on the thickness of the top layer. A thick top layer results in a larger hydraulic head compared to a thin top layer. A larger hydraulic resistance for a thick top layer causes this. In contrast, a thin top layer has a tendency to breach with a lower hydraulic head. This explains the dependency of the hydraulic head on the width of the channel belt, where the top layer is relatively thin. A large width results in more water seeping through the thin top layer. The hydraulic head decreases as the width of the channel belt increases. Channel belts with limited width result in more days with a risk for breaching of the top layer, while this risk for wide channel belts covers a larger area. Taal [2015] concluded that most observations of piping are found at disturbances in the subsurface like trees, fences and ditches. Therefore, wide channel belts form a larger risk for piping than narrow channel belts because more disturbances in the subsurface can be expected in a larger area.

Another investigated scenario is a channel belt with a limited incision in the underlying sand body. The hydraulic head is largest at the location of the incision. Groundwater flows from the Pleistocene sand body into the channel belt. This results in a decreasing hydraulic head in the channel belt, as the distance away from the incision becomes larger. The Sellmeijer formula does not consider this mechanism.

Figure 5.1 shows the area with a risk for piping plotted on the results of this research (Figure 4.3d and Figure 4.5c). The results of the Sellmeijer formula used for this figure are number one, four and seven from Table 4.1. These contain the smallest grain size and therefore the largest required seepage length. The available seepage length is 100 meters. The combination of a top layer thickness of one meter and a 35 meters thick aquifer results in 299 meters required seepage length. This length regards for the full width of the channel belt, when the channel belt incises the underlying sand body entirely (Figure 5.1a). Using the properties of a channel belt that is not incised in the underlying sand body (D = 4 meters) results in 92 meters required seepage length. The thickness of the aquifer (D) varies for the schematization of a

partly incised channel belt. This schematization of the subsurface results in, when following the strict method of Sellmeijer, no risk for piping between the edge of the incision and the boundary of the channel belt because the thickness of the channel belt is four meters. Comparing this with the risk for breaching of the top layer leads to contradictory results. The Sellmeijer formula considers a straight line between the river and the polder because it is limited by its two-dimensional approach. Therefore, the breached top layer of the channel belt that is located beside the incision, but within the required seepage length of 299 meters, is not considered by the Sellmeijer formula (red circles in Figure 5.1b). At these locations, the top layer can breach, which could result in erosion. This erosion is expected in the direction of the largest hydraulic head [Förster et al., 2012] towards the incision of the channel belt, not in the direction of the river.

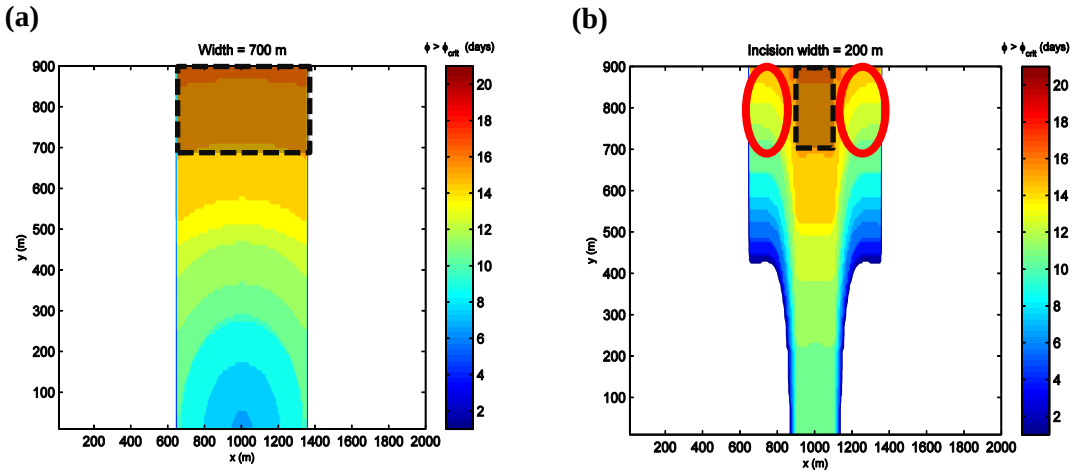

Figure 5.1 Results of the Sellmeijer formula plotted on the results of calculations with iMOD (area marked in black).

The complex schematizations of the subsurface used in this research contain variations in top layer thickness, channel belt thickness, permeability and incision width. The risk for breaching of the top layer is largest at the locations with a top layer thickness of one meter. In addition, the hydraulic head is influenced mainly by groundwater entering the channel belt from the underlying sand body. Groundwater entering the channel belt directly from the river influences the hydraulic head less significant. A comparison with the Sellmeijer formula does not lead to useful results. The channel belt contains too many variations in the input parameters for the Sellmeijer formula. In addition, the direction of the erosion is not expected towards the river, but in the direction of the incision. Other findings of the results are:

- The risk for breaching of the top layer is largest at the edge of the channel belt. Here, the hydraulic head has a large dependency on the hydraulic head induced by a thick top layer. This could lead to accelerated erosion of the aquifer. The Sellmeijer formula only uses the critical hydraulic head and does not consider this dependency.

- The risk of breaching of the top layer is lower for channel belts that are isolated from the underlying sand body. The results of the Sellmeijer formula show that piping will not occur, which is caused by the limited thickness of the isolated channel belt. This only accounts for isolated channel belts because the groundwater flow is only induced by the hydraulic connection with the river.

The models used in this research are based on field data from a study area in the Rhine-Meuse delta. This data is used to choose the right input values for the parameters to create the schematizations. iMOD uses two parameters that are not present in the dataset. The storage coefficient is based on suggested values from literature. The storage coefficient of the top layer has a large influence on groundwater flow. Additional (literature) research to improve the parameter estimations of this layer will lead to better predictions of hydraulic head. Another assumed parameter is the conductance of the river. For this research, a worst-case value is used. This assumes that water from the river can flow easily into the aquifer, resulting in a high hydraulic head. Additional fieldwork will give more information about the conductance, which leads to better predictions of the hydraulic head.

Part of the aim of the research was formulating an approach for further research. The next steps that should be taken to improve the understanding of piping with three-dimensional groundwater models are explained below. Breaching of the top layer is for this research investigated by making a comparison between the critical hydraulic head and the calculated hydraulic head. The effect of a breached top layer on the behavior of groundwater flow is not investigated. iMOD provides a tool to implement a well into a model. The principle of a well is equal to a breached top layer: groundwater is able to flow from the aquifer towards the surface. The most useful aspects to investigate are the hydraulic head at the location of the well and the influence on the hydraulic head in the surrounding area. The discharges through the well and well size are expected to have large influence on the hydraulic head. iMOD is able to calculate flow directions. This tool is useful to investigate the three-dimensional behavior of groundwater flow. Groundwater flow directly beneath the top layer and in the direction from the river towards the well is most relevant for piping. This could be the route of erosion. Furthermore, this method can exclude situations with a risk for piping. The flow direction and therefore erosion could move away from the river too. This influences the stability of the dike less. Additional research with conceptual schematizations in iMOD could prove this expectation.

Meandering river deposits contain large variations in grain size. This is explained in chapter 2.2. This research only implemented variations in permeability in the models, with the

assumption that all layers are permeable. Impermeable lithological units like reactivation surfaces of point bars will result in differences in horizontal and vertical permeability. It is recommended to investigate this feature of meandering river deposits because the influence on groundwater flow is expected to be large.

6 Conclusion

This study proves that three-dimensional groundwater models like iMOD are a useful tool for investigating the behavior of groundwater flow underneath dikes in heterogeneous subsurfaces. Groundwater flow from the river into the aquifer towards the polder is calculated successfully with iMOD. The calculated hydraulic head shows explainable dependencies on three-dimensional variations in the subsurface. The largest dependency is on variations in top layer thickness and the thickness of the aquifers. Most parameters that are used to schematize subsurface and its properties came from existing datasets that are collected for the current method to calculate piping. This contributes to the applicability and reliability of the calculations in iMOD.

The risk in days for breaching of the top layer during a flood wave is set as an indicator for the risk of piping. This risk depends on the properties of the channel belt. Situations with a narrow channel belt result in more risk (day) for breaching of the top layer. On the other hand, this risk for breaching of the top layer covers a larger area for wide channel belts, while the number of days of this risk is less.

For partly incised channel belts, the risk for piping is larger than the traditional method for calculating piping suggests. The aquifer thickness is significantly less at the isolated part of the channel belt and therefore the calculations with Sellmeijer result in small required seepage lengths. At these locations, the groundwater flow is not induced by the connection of the channel belt with the river, but by the incision nearby. A two-dimensional approach cannot take this into consideration. The results from three-dimensional calculations show a risk for breaching of the top layer, located at the isolated part of the channel belt within the distance of the required seepage length. This will result in three-dimensional development of piping.

This research forms the foundation for further research to three-dimensional modeling of groundwater underneath dikes. Recommendations are formulated based on the results of this research and the possibilities of iMOD. The first steps that should be made are:

- investigating the influence of a breached top layer on the hydraulic head;
- investigating the directions of groundwater flow from the river towards a breach in the top layer through a heterogeneous subsurface.

7 References

ARCADIS. (2012). Consequentie-analyse aangepaste pipingregel.

Batu, V., (1998). *Aquifer Hydraulics: A Comprehensive Guide to Hydrogeologic Data Analysis*, John Wiley & Sons, New York, 727p.

Berendsen, H.J.A. (2008). *De vorming van het land (vijfde druk).* Assen: Van Gorcum.

Bligh, W.G. (1910). *Dams Barrages and Weirs on Porous Foundations*, Engineering News, p. 708.

Bridge, J. (2003). *Rivers and Floodplains - Forms, Processes and Sedimentary Record.* Blackwell Science Ltd, Oxford, UK, 504 pp. ISBN 0632064897.

Brunner, P., & Simmons, C. T. (2012). *HydroGeoSphere: A Fully Integrated, Physically Based Hydrological Model.* Ground Water, 50(2), 170–176. doi:10.1111/j.1745-6584.2011.00882.x

Busschers, F.S. and Weerts, H.J.T. (2003). *Kreftenheye. In: Lithostratigrafische Nomenclator van de Ondiepe Ondergrond*. Retrieved 18-05-2015 from https://www.dinoloket.nl/formatie-van-kreftenheye.

Cohen, K.M., Stouhamer, E., Hoek, W.Z., Berendsen, H.J.A., & Kempen, H.F.J. (2009). *Zand in banen*, 3e druk. Arnhem: Provincie Gelderland.

K.M. Cohen, E. Stouthamer, H.J. Pierik, A.H. Geurts (2012) *Digitaal Basisbestand Paleogeografie van de Rijn-Maas Delta / Rhine-Meuse Delta Studies' Digital Basemap for Delta Evolution and Palaeogeography. Dept. Physical Geography. Utrecht University. Digital Dataset.* http://dx.doi.org/10.17026/dans-x7g-sjtw

Domenico, P.A. and M.D. Mifflin, (1965). *Water from low-permeability sediments and land subsidence*, Water Resources Research, vol. 1, no. 4., pp. 563-576.

Förster, U., van den Ham, G., Calle, E., & Kruse, G. (2012). *Onderzoeksrapport Zandmeevoerende Wellen.*

Gibling, M. R. (2006). *Width and Thickness of Fluvial Channel Bodies and Valley Fills in the Geological Record: A Literature Compilation and Classification.* Journal of Sedimentary Research, 76(5), 731–770. doi:10.2110/jsr.2006.060

Glenn M. Duffield (2015*).* *Representative Values of Hydraulic Properties [online]*. HydroSOLVE, inc. http://www.aqtesolv.com/aquifer-tests/aquifer_properties.htm [visit date: 11/2015]

Harbaugh, A. W. (2005). *MODFLOW-2005, the US Geological Survey modular ground-water model: The ground-water flow process* (pp. 6-A16). Reston, VA, USA: US Department of the Interior, US Geological Survey.

Heath, R.C., (1983). *Basic ground-water hydrology*, U.S. Geological Survey Water-Supply Paper 2220,86p.

Kanning, W. (2012). *The Weakest Link.* Academic Medicine (Vol. 4). doi:10.1097/00001888-192907000-00003

Knoeff, H., Sellmeijer, J. B., Lopez, J., & Luijendijk, S. (2009). *SBW Piping - Hervalidatie piping. VNK (2015).* De veiligheid van Nederland in kaart. Rijkswaterstaat Projectbureau VNK. Document HB 2540621, 120 p.

Koelewijn, A.R. (2009): *SBW Hervalidatie Piping, E. Evaluatie 0,3d rekenregel.* Rapport 1001453-002-GEO-0002, Deltares.

Koopmans, R., & Van den Berg, S. (2015). *Pipingonderzoek dijkring 43, D70 en kD bepaling.* POV piping

Lane. E.W. (1935). *Security from Under-Seepage Masonry Dams on Earth Foundations*, Transactions ASCE, Vol. 100 , Paper no. 1919

Lewin, J., & Macklin, M. G. (2003*).* *Preservation potential for late quaternary river alluvium.* Journal of Quaternary Science, 18(2), 107–120. doi:10.1002/jqs.738

Lohman, S.W., (1972). *Ground-water hydraulics*, U.S. Geological Survey Prof. Paper 708, 70p.

Lunt, I. a., Bridge, J. S., & Tye, R. S. (2004). *A quantitative, three-dimensional depositional model of gravelly braided rivers. Sedimentology*, 51(3), 377–414. doi:10.1111/j.1365-3091.2004.00627.x

Maill, A..M. (1996). *The Geology of Fluvial Deposits, Sedimentary Facies, Basin Analysis and Petroleum Geology.* Springer.

Ministerie van Verkeer en Waterstaat (2006). *Hydraulische randvoorwaarden primaire waterkeringen voor de derde toetsronde 2006-2011 (HR 2006).*

Ministery of Transport Public works and Water Management. (2006). *Voorschrift Toetsen op Veiligheid Primaire Waterkeringen.*

Prothero, D.R. and Schwab, F. (1996). *Sedimentary Geology: An introduction to sedimentary rocks and stratigraphy.* New York : W. H. Freeman and Company

Rijkswaterstaat Projectbureau VNK (2015) *Veiligheid van Nederland in kaart.* HB 2540621

Schweckendiek, T., Vrouwenvelder, a. C. W. M., & Calle, E. O. F. (2014). *Updating piping reliability with field performance observations.* Structural Safety, 47, 13–23. doi:10.1016/j.strusafe.2013.10.002

Sellmeijer, J. B. (1989). *On the mechanism of piping under impervious structures.* Repository. Tudelft.Nl, 116. Retrieved from http://repository.tudelft.nl/assets/uuid:7f3c5919-1b37-4de9-a552-1f6e900eeaad/TR diss 1670(1)

Sellmeijer, J. B. (2006). *Numerical computation of seepage erosion below dams (piping).* Third International Conference on Scour and Erosion, 596–601.

Sellmeijer, H., de la Cruz, J. L., van Beek, V. M., & Knoeff, H. (2011). *Fine-tuning of the backward erosion piping model through small-scale, medium-scale and IJkdijk experiments.* European Journal of Environmental and Civil Engineering, 15(8), 1139–1154. doi:10.1080/19648189.2011.9714845

Slot, A.F.M., Hertogh, K. (2015). *Pipingonderzoek dijkring 43 IJzendoorn*

TAW. (1985). *Leidraad voor het ontwerpen van rivierdijken.* 's-Gravenhage: Staatuitgeverij.

Thonus et al (2005). *Review koploper resultaten VNK, faalmechanisme piping*, HKV-lijn in water, rapportnummer PR761,10 april 2004

Toonen, W. H. J., Kleinhans, M. G., & Cohen, K. M. (2012). *Sedimentary architecture of abandoned channel fills*. Earth Surface Processes and Landforms, 37(4), 459–472. doi:10.1002/esp.3189

Vandenboer, K., Bezuijen, A., & van Beek, V. M. (2015). *3D character of backward erosion piping : Small-scale experiments.* Scour and Erosion, 1, 81–86.

Van der Meer, M. T., Niemeijer, J., Post, W. J., & Heemstra, J. (2004). *Technisch rapport waterspanningen bij dijken Waterkeringen (TAW).* Rijkswaterstaat, DWW.

Van Dijk, W. M., Van De Lageweg, W. I., & Kleinhans, M. G. (2012). *Experimental meandering river with chute cutoffs.* Journal of Geophysical Research: Earth Surface, 117(3), 1–18. doi:10.1029/2011JF002314

Vermeulen, P.T.M. and Minnema, B., (2015). *IMOD User Manual version 3.01*, Deltares 41985, 580p.

Vrijling, J. K., Kok, M., Calle, E. O. F., Epema, W. G., Van der Meer, M. T., Van den Berg, P., & Schweckendiek, T. (2010). *Piping: Realiteit of Rekenfout ?*

Westerhoff, W.E. (2003). *Sterksel. In: Lithostratigrafische Nomenclator van de Ondiepe Ondergrond.* Retrieved 18-05-2015 from https://www.dinoloket.nl/formatie-van-sterksel

Appendix I: Results of the pumping tests

Slot and Hertogh [2015] determined the values for permeability for the Holocene and Pleistocene deposists (Table A1). The weigthed average for permeability of all layers is 52.0 m/d. For the Holocene deposits (nr 2 and 3), the weighted average is 10 m/d and for the Pleistocene deposits (nr 4 – nr 12) is 59.0 m/d.

Table A1 Results of the pumping test executed by Slot and Hertogh [2015].

nr	**layer**	**thickness (m)**	**head (m+NAP)**	**kD (m^2/d)**	**k (m/d)**
	surface		6		
1	top layer	1	5		0,01
2	sand, moderate coarse	2,8	2,2	40	10
3	sand, moderate fine	2,4	-0,2	40	10
4	sand, very coarse	2,9	-3,1	46	16
5	gravel, fine	0,8	-3,9	84	105
6	sand, extremely coarse	4,2	-8,1	219	52
7	sand, very coarse	3,9	-12	92	24
8	gravel, fine	4	-16	421	105
9	sand, extremely coarse	1	-17	37	37
10	sand, very coarse	4	-21	140	35
11	sand, extremely coarse	3	-24	92	31
12	gravel, fine	6	-30	632	105
13	bottom				

Appendix II: RUN-files

The RUN-files are stored on the supplied disk

Appendix III: IDV-files

The IDV-files are stored on the supplied disk

Appendix IV: Matlab-files

The Matlab-files are stored on the supplied disk

Appendix V: Calculations with the Sellmeijer formula

The calculations are stored on the supplied disk